To my family

CELL-FREE SYHTHETIC BIOLOGY ENABLED RNA TOEHOLD SWITCH SYSTEM FOR INFLUENZA VIRUSES

A THESIS SUBMITTED TO THE GRADUATE SCHOOL OF

ENGINEERING AND SCIENCE

OF BILKENT UNIVERSITY

IN PARTIAL FULFILLMENT OF THE REQUIREMENTS FOR

THE DEGREE OF

MASTER OF SCIENCE

IN

MATERIALS SCIENCE AND NANOTECHNOLOGY

By

Abdurahman ATILLA

AUGUST 2025

CELL-FREE SYNTHETIC BIOLOGY ENABLED RNA TOEHOLD SWITCH SYSTEM FOR INFLUENZA VIRUSES

By Abdurahman Atilla

August 2025

We certify that we have read this dissertation and that in our opinion it is full adequate, in scope and in quality, as a thesis for the degree of Master of Science.

Urartu Özgür Şafak Şeker
(Advisor)

Seymur Jahangirov

Hüseyin Burak Çalışkan

Approved for the Graduate School of Engineering and Science:

Orhan Arıkan

Director of the Graduate School

ABSTRACT

CELL-FREE SYHTHETIC BIOLOGY ENABLED RNA TOEHOLD SWITCH SYSTEM FOR INFLUENZA VIRUSES

Abdurahman Atilla

M.Sc in Materials Science and Nanotechnology

August, 2025

Influenza A H1N1 continues to pose a major public health threat due to its rapid transmission and capacity to cause seasonal epidemics and pandemic outbreaks. Rapid, accurate, and cost-effective diagnostic approaches are essential for timely intervention and control of viral spread. In this study, we present a synthetic biology-based diagnostic strategy that employs programmable RNA-based regulatory elements, known as toehold switches, to selectively detect Influenza A H1N1 viral RNA sequences. These switches were designed to remain translationally inactive in the absence of the viral RNA and to activate protein expression upon specific sequence recognition.

The initial switch designs were computationally generated and analyzed using thermodynamic modeling tools such as NUPACK and RNAfold, allowing for assessment of structural stability and identification of high-entropy regions that could affect translation. Particular attention was given to the accessibility of the ribosome binding site and start codon regions, as local structural hindrances in these

areas were found to correlate with poor performance. Based on the entropy profiles and free energy distributions, selected constructs were subjected to rational sequence redesign to enhance conformational accessibility and minimize undesired leakiness.

These optimized switches were then cloned into T7 promoter-driven plasmids and tested through in vitro transcription–translation reactions. The resulting GFP-based fluorescence measurements allowed us to quantitatively compare expression levels in the presence and absence of the target RNA. Experimental data showed that optimized switch designs provided significantly higher signal-to-noise ratios, reduced background expression, and more consistent fold-change values across replicates compared to their unoptimized counterparts.

Overall, this study demonstrates the potential of rationally engineered RNA-based switches as a modular, programmable, and low-cost diagnostic platform for Influenza A H1N1. Moreover, the design framework established here can be generalized to support the development of similar RNA-sensing tools for other viral pathogens.

Keywords: Synthetic biology, Diagnostics, Infectious disease, Toehold Switch

ÖZET

İNFLUENZA VİRÜSLERİNE YÖNELİK HÜCRESİZ SENTETİK BİYOLOJİ DESTEKLİ RNA TOEHOLD SWİTCH TANI SİSTEMİ

Abdurahman Atilla

Malzeme Bilimi ve Nanoteknoloji, Yüksek Lisans

Tez Danışmanı: Urartu Özgür Şafak Şeker

Ağustos, 2025

Influenza A H1N1, hızlı bulaşma kabiliyeti ve mevsimsel salgınlar ile pandemilere yol açabilme potansiyeli nedeniyle küresel düzeyde önemli bir halk sağlığı tehdidi olmaya devam etmektedir. Bu virüsle etkin şekilde mücadele edebilmek için, hızlı, doğru ve düşük maliyetli tanı yöntemlerinin geliştirilmesi büyük önem taşımaktadır. Bu çalışmada, Influenza A H1N1 virüsüne özgü RNA dizilerini seçici olarak tanıyabilen programlanabilir RNA tabanlı düzenleyici elemanlar olan toehold switch'lere dayalı sentetik biyoloji temelli bir tanı stratejisi sunulmuştur. Bu sistem, hedef viral RNA bulunmadığında translasyonel olarak baskılanan, ancak özgül diziyi tanıdığında protein ekspresyonunu aktive eden tasarımlara dayanmaktadır.

İlk switch tasarımları, yapısal kararlılık ve fonksiyonel bölgelerin erişilebilirliğini değerlendirmek amacıyla NUPACK ve RNAfold gibi termodinamik modelleme araçları kullanılarak oluşturulmuş ve analiz edilmiştir. Özellikle ribozom bağlanma

bölgesi (RBS) ve başlangıç kodonunun çevresindeki yapısal engellerin düşük performansla ilişkili olduğu belirlenmiş ve entropi profilleri ile serbest enerji dağılımları temel alınarak rasyonel dizayn iyileştirmeleri yapılmıştır.

Optimize edilen switch dizileri T7 promotörü altında ekspresyon sağlayan plazmitlere klonlanarak, in vitro transkripsiyon-translasyon reaksiyonları ile test edilmiştir. Elde edilen GFP tabanlı floresan ölçümleri, hedef RNA'nın varlığı ve yokluğu koşullarındaki gen ekspresyon düzeylerinin nicel karşılaştırılmasına olanak sağlamıştır. Elde edilen deneysel veriler, optimize edilmiş switch tasarımlarının daha yüksek sinyal-gürültü oranları, daha düşük bazal ekspresyon ve tekrarlanabilir katlanma değerleri sağladığını ortaya koymuştur.

Genel olarak bu çalışma, rasyonel olarak tasarlanmış RNA tabanlı switch'lerin Influenza A H1N1 için modüler, programlanabilir ve düşük maliyetli bir tanı platformu olarak kullanılabileceğini göstermektedir. Ayrıca burada ortaya konan tasarım yaklaşımı, diğer viral patojenlerin tanısı için benzer RNA algılayıcı sistemlerin geliştirilmesinde de genel geçer bir çerçeve sunmaktadır.

Anahtar Kelimeler: Sentetik biyoloji, Tanı Yöntemi, Enfeksiyon Hastalıkları, Toehold Sensör

ACKNOWLEDGEMENTS

First and foremost, I would like to thank Asst. Prof. Urartu Özgür Şafak Şeker for giving me the opportunity to join his research group. I first met him during summer internship, which sparked my initial interest in the field. I appreciate his contributions to my academic growth and the chance to carry out my research under his supervision.

I would also like to extend my heartfelt thanks to the members of my thesis jury, Assoc. Prof. Seymur Jahangirov, and Asst. Prof. Hüseyin Burak Çalışkan. Their insightful feedback, constructive criticism, and thoughtful questions during my defense have been invaluable. I am deeply grateful for the time and effort they dedicated to reviewing my work and their contributions to my academic growth.

To the current members of the Synthetic Biosystems Laboratory, working with such a friendly and inspiring group of people has been an incredible experience. I especially want to thank Gizem Makas for her kindness, assistance, and support. I would like to give special thanks to some members of the SBL. Nazlıcan Tunç, for being both a confidante and someone who never failed to support me, even when offering criticism. Her presence was a steady source of comfort throughout. Damla Albayrak, for being a quiet yet steady presence in the lab, never loud, but always grounding. In a galaxy of deadlines and failed experiments, she reminded me that not every battle needs a lightsaber. Senem Şen, for making me feel the presence of an older sister, something I never had but deeply valued throughout this journey. Aslı Doğruer, for the sweet little conversations during experiments that made long lab days more bearable. Cem Dirse Polat, for the beautiful assists on the field, best no. 10 I have ever played with. Derin Akman and Ece Avcı, for their support and sweet

little chats during this process. Cemile Elif Özçelik, for her support and guidance ever since my internship days.

Finally, I would like to extend my heartfelt thanks to my family. You believed in me even when I couldn't believe in myself. I also want to thank everyone who has helped make Ankara a more livable place. And of course, special thanks to my fluffy friend Bulut, for being a source of energy and comfort. Thank you all for always being there for me. I wouldn’t have made it this far without your support.

Contents

LIST OF TABLES

LIST OF FIGURES

CHAPTER I: INTRODUCTION

1.1. Influenza A H1N1

Influenza viruses are among the most important pathogens that affect people all over the world. Influenza viruses are part of the Orthomyxoviridae family and have segmented, negative-sense single stranded RNA genomes. Among the three types that infect humans – Influenza A, B, and C- Influenza A viruses are the most likely to cause pandemics because of its wide host range, high rate of mutation, and ability to shift and drift antigens, the influenza A virus is the most virulent and epidemiologically significant. In addition, to allowing the virus to evade host immune responses, these evolutionary dynamics make vaccine development and public health preparedness more challenging [1].

Based on the antigenic characteristics of two glycoproteins on their surface, hemagglutinin (HA) neuraminidase (NA), influenza A viruses are further divided into subtypes. There are currently 18 HA and 11 NA subtypes known to exist, and different combinations of these subtypes are found in swine, human, and bird populations. The H1N1 genome is composed of eight RNA segments, as shown in figure 1, each of which codes for one or more viral proteins required for replication, host adaptation, and immune evasion [2, 3].

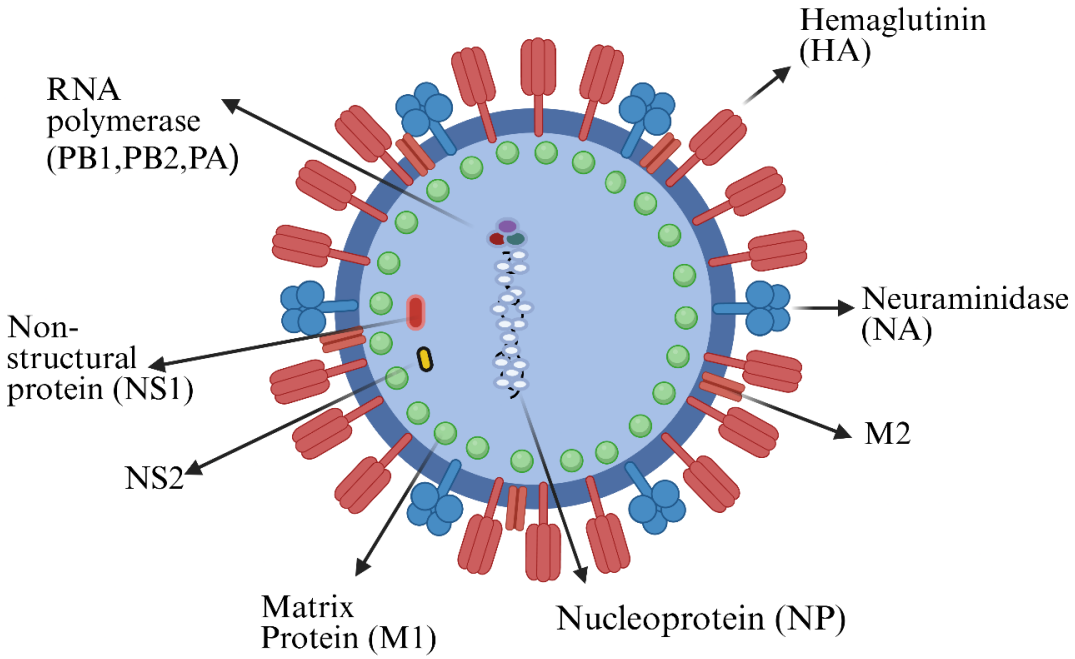

Figure 1: Schematic representation of the Influenza A virus structure, highlighting major structural and non-structural proteins including hemagglutinin (HA), neuraminidase (NA), RNA polymerase complex (PB1, PB2, PA), matrix proteins (M1, M2), nucleoprotein (NP), and non-structural proteins (NS1, NS2). Illustration is created using BioRender.com.

These segments are as follows:

- Segment 1 – Polymerase Basic Protein 2 (PB2): involved in the start of transcription via cap binding.
- Segment 2 – Polymerase Basic Protein 1 (PB1): central catalytic subunit of the RNA-dependent RNA polymerase.
- Segment 3 – Polymerase Acidic Protein (PA): has the ability to support polymerase assembly and show endonuclease activity.
- Segment 4 – Hemagglutinin (HA): facilitates viral entry by binding to host cell receptors.

- Segment 5 – Nucleoprotein (NP): encapsidates the viral RNA, essential for genome packaging and replication.
- Segment 6 – Neuraminidase (NA): enables viral release from host cells by cleaving sialic acid residues.
- Segment 7 – Matrix Proteins (M1/M2): M1 supports virion structure; M2 functions as an ion channel during viral uncoating.
- Segment 8 – Nonstructural Proteins (NS1/NS2): Each encoding one or more viral proteins necessary for replication, host adaptation, and immune evasion, NS1 suppresses host immune responses, while NS2 aids in the nuclear export of viral ribonucleoprotein (RNP).

Influenza A H1N1 has a notable history. The virus subtype was identified retrospectively as a potential contributor to the 1918 ‘Spanish flu’ pandemic, one of the deadliest disease outbreaks in modern history which resulted in an estimated 50 million deaths worldwide, was caused by a strain of the H1N1 subtype. However, influenza viruses were not identified or isolated in the laboratory until the 1930s. In 1933, Smith, Andrewes, and Laidlaw were able to separate the first human Influenza A virus in the United Kingdom. In 1940s, scientists were able to tell different types of influenza virus apart by looking at their surface proteins, such as hemagglutinin (HA) and neuraminidase (NA). This finding led to the classification of H1N1 as a unique subtype. Since then, there have been many different types of H1N1 around the world, both in seasonal and pandemic forms [4, 5].

The most recent major emergence of H1N1 occurred in April 2009, when the Centers for Disease Control and Prevention (CDC) discovered an unusual

influenza A virus in two California children. A novel triple-reassortant strain with gene segments from avian, swine, and human influenza viruses was discovered through genetic analysis. The World Health Organization (WHO) declared this variation, known as pdmH1N1, a pandemic due to its rapid global spread. An estimated 1.4 billion people were infected during the outbreak, and over 200,000 deaths were reported globally [6].

The clinical symptoms of an H1N1 infection are often similar to those of other influenza strains and include fever, cough, sore throat, nasal congestion, headache, fatigue, and myalgia. The 2009 strain was associated with a usually large percentage of severe cases in young adults, pregnant women, and individuals with underlying medical conditions, which is different from the typical age distribution observed in seasonal influenza. Complications such as viral pneumonia, acute respiratory distress syndrome (ARDS), and multi-organ failure can require intensive care and mechanical ventilation in severe cases [6, 7].

H1N1 is mainly spread by airborne particles released during speaking, sneezing, or coughing. Additionally, environmental surfaces and direct contact with contaminated surfaces aid in the spread of the disease, especially in crowded or enclosed spaces like schools, military barracks, and medical facilities. Containment efforts are complicated by the virus's one to four day incubation period and the possibility that an individual may be contagious before symptoms appear [8]. After inhalation of respiratory droplets containing influenza A H1N1 virions, the virus primarily targets epithelial cells lining the upper respiratory tract. The first adhesion occurs through the viral surface glycoprotein hemagglutinin (HA), which specifically recognizes

and binds to sialic acid residues found in host cell membrane glycoproteins. This binding facilitates viral adhesion and determines host specificity and tissue tropism [5].

Following binding, the virus is internalized into the host cell via receptor-mediated endocytosis. Once inside the endosome, a decrease in pH triggers a conformational change in HA, exposing the fusion peptide. This facilitates fusion between the viral envelope and the endosomal membrane, releasing viral ribonucleoproteins (VRNPs) into the cytoplasm [7] .

The vRNPs are then transported into the nucleus, which is somewhat unusual for an RNA virus. Inside the nucleus, the viral RNA-dependent RNA polymerase initiates the transcription of viral mRNAs by using capped pre-mRNAs of the host cell as primers—a mechanism known as cap-snatching. In parallel, complementary RNA (cRNA) intermediates are synthesized for genome replication.

The viral mRNAs are exported to the cytoplasm for translation, leading to the synthesis of viral proteins such as hemagglutinin (HA), neuraminidase (NA), matrix proteins (M1, M2), and nucleoproteins. These proteins are then properly processed and trafficked: surface proteins are directed to the host plasma membrane, while nucleoproteins re-enter the nucleus to assist in assembling new vRNP complexes [2].

As the replication cycle progresses, newly synthesized vRNPs are exported from the nucleus and transported to the plasma membrane, where they interact with viral envelope proteins. Viral assembly takes place at the membrane, followed by the budding of new virions from the cell surface. At

this stage, neuraminidase plays a critical role by cleaving sialic acid residues to prevent self-aggregation and facilitate viral release [1, 8].

This entire process is rapid and efficient, typically resulting in high viral loads and significant cell damage, which contributes to the clinical symptoms of influenza infection such as fever, sore throat, and cough [6].

Effective management of influenza outbreaks depends on quick and accurate diagnosis. The reverse transcription polymerase chain reaction (RT-PCR) remains the gold standard for detecting influenza A H1N1 due to high sensitivity and specificity. However, RT-PCR requires specialized personnel, cold-chain logistics, and advanced lab equipment, resources that may not be readily available in low-income or field settings. Rapid antigen detection tests (RADTs) and immunofluorescence assays are examples of alternative diagnostic techniques that offer faster results, but they usually have lower sensitivity, especially in the early stages of infection [9].

There is an urgent need for new, cheap, and easy-to-use solutions that can be used in the field because the flu virus is still a threat and current ways of diagnosing and treating it are not good enough. Advancements in synthetic biology, particularly cell-free transcription-translation (TX-TL) systems and toehold switch-based RNA sensors, offer a promising avenue for next-generation diagnostics. These systems are not only easy to program and modular, but they also work with ambient storage and freeze-drying. This makes them great for emergencies or when resources are limited [10].

1.2. Toehold Switch-Based Diagnostics

Toehold switches are synthetic RNA-based genetic elements that regulate gene expression at the translational level. They are one of the most advanced and useful tools in the quickly growing field of synthetic biology. In 2014, Green et al. were the first to provide information about these molecular switches. They are riboregulators that act as very specific biosensors. They can find different RNA sequences and turn that detection into a measurable output, such as fluorescence or colorimetric signals. Toehold switches let you detect and amplify signals using only RNA, which is different from other RNA sensing methods that usually need enzymes, antibodies, or complicated equipment [11, 12].

A toehold switch is made up of a synthetic RNA hairpin loop that holds the start codon and ribosome binding site (RBS) in a stem-loop structure. This type of folding stops gene expression by keeping ribosomes from getting to it. But when a piece of viral RNA or another RNA that is complementary to the 5' toehold region binds to it, the hairpin becomes unstable. This opens it up and lets the ribosome attach and start the translation. The modular switch-on mechanism is very precise, so the system can tell the difference between different single-nucleotide variants in the target sequence[11, 13, 14] .

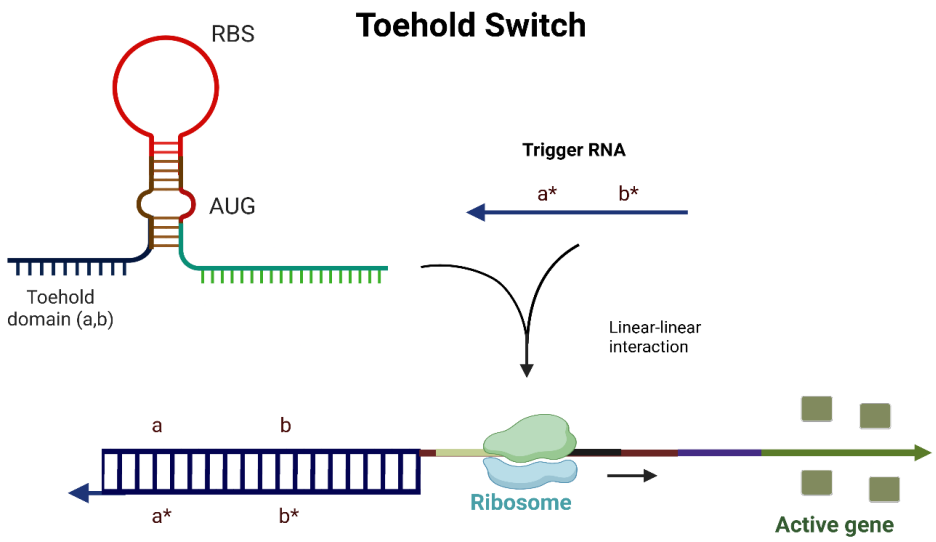

Figure 2: Schematic representation of a toehold switch mechanism. The toehold switch has a structured RNA hairpin that hides the ribosome binding site (RBS) and the start codon (AUG). This stops translation. When a certain trigger RNA binds to the hairpin through complementary domains (a*, b*), the hairpin unfolds through a linear-linear interaction. This exposes the RBS and lets the ribosome access the downstream active gene for translation. Illustration is created using BioRender.com.

Toehold switches are robust because they can be programmed and are stable in terms of thermodynamics. NUPACK, ViennaRNA, and RNAfold are examples of computational tools that can improve switch structures by lowering off-target binding and making the closed-state conformation more energetically favorable. These tools make it easy to guess about secondary structures and binding kinetics, which makes it easy to repeat and improve

the design process. Toehold switches can also be used in more than one reaction at the same time, which lets you find more than one target at once. This is a big plus for tests that look for co-infections or different types of diseases [15, 16].

The first time toehold switches were used in a real-world diagnostic setting was during the Zika virus outbreak. They were made with synthetic RNA sequences. Researchers made paper-based sensors that could find Zika viral RNA in clinical samples in less than three hours. These sensors do not need power, refrigeration, or lots of complicated infrastructure. This project, done by the same group that made the technology, was a turning point for using programmable biosensors to respond to epidemics [13]. Shortly after COVID-19 started, toehold-based biosensors were quickly modified to detect SARS-CoV-2 RNA with high specificity and sensitivity, like RT-qPCR [17, 18].

These examples showed even more how easy and cheap it is to use toehold-based diagnostics. Toehold switches are a great way to find the Influenza A H1N1 virus for many reasons. It is difficult to monitor influenza viruses using static diagnostic methods due to their rapid mutation rates and diverse antigenic profiles. Toehold switches can be quickly rebuilt in silico to target new strains by finding parts of viral RNA that are only found in the target population and not in other circulating subtypes [9].

Toehold switches have technological benefits, but they can also be used in a number of readout platforms. For example, reporter enzymes like lacZ (β-

galactosidase) can be used to make outputs that change color. When these enzymes touch a substrate, they change color. Fluorescence outputs can be made with green fluorescent protein (GFP) or one of its variants. This makes it possible to take measurements that are accurate [19].

The unique combination of programmability, portability, specificity, and modularity makes toehold switches an important part of the next-generation molecular diagnostics. Using them to find H1N1 viral RNA, especially on a synthetic, cell-free platform, is a powerful, easy, and scalable way to solve the problems that influenza viruses and other new pathogens pose for diagnosis.

1.3. Aim of the Study

The primary objective of this study is to use synthetic biology to find a new and simple way to find the influenza A H1N1 virus. The main goal is to develop and utilize a cell-free diagnostic tool that relies on toehold switches, which are RNA-based regulatory elements. These manufactured riboregulators to only respond to certain viral RNA sequences, which allows applying a very targeted detection method.

A cell-free system has been selected because it is cheap and adaptable, especially when compared to traditional molecular diagnostic methods that often require expensive lab equipment, skilled staff, and cold-chain logistics. A cell-free setup, on the other hand, can be frozen or kept at room

temperature. This makes it useful in the field or when there are not many resources available [20].

The goal of the project is to show that synthetic regulatory circuits can be changed to meet real-world diagnostic needs by making toehold switches that respond to preserved genetic regions of the H1N1 subtype. The final goal is to help make biosensing tools that are cheap and portable so that they can be used to find more respiratory viruses in the future [21], [22].

CHAPTER II: MATERIALS AND METHODS

2.1 Cell Strains, Growth, Transformation, and Cell Maintenance

The coli *E.coli* DH5α strain was used for all the cloning experiments because it has a strong insert integrity and high DNA yield. The *E.coli* BL21 DE3 strain was used to make recombinant proteins. At -80°C, all cell stocks were kept in 25% glycerol in Lysogeny Broth (LB) solution (recipe given in Supplementary Information E, Table E.1).

Plasmids were introduced into the bacterial strains mentioned above via chemical transformation. To prepare E. coli DH5α and E. coli BL21 (DE3) cells for transformation via chemical treatment, overnight cultures were initiated from -80°C glycerol stocks in LB medium containing appropriate antibiotics. After that, overnight cultures were diluted 1:100 and cultured in antibiotics-containing LB media until their OD600 reached 0.4 to 0.6. They were then chilled on ice for ten minutes. Following 10 minutes at 4°C and 3000 x g centrifugation, the cells were separated from the supernatant. The remaining cell pellet was reconstituted at a 1:10 dilution in Transformation and Storage (TSS) Buffer (recipe in Supplementary Information E, Table E.2). -80°C was used to store 100 µL aliquots of chemically competent cell solution for upcoming transformations.

100 nanogram (ng) of the chosen plasmid was added after the chemically competent cells had thawed on ice, and the mixture was then incubated on ice for 30 minutes. After 45 seconds of heat shock at 42°C, the cells were immediately placed on ice for two minutes to enable plasmid entry through the pores that had been opened. Cells were incubated for 45 minutes at 37°C and 200 rpm in a shaking incubator after 300 µL of LB was added. For five minutes, cells were centrifuged at 8000 rpm. The remaining cell pellet was resuspended in the 100 µL supernatant, while the rest of the supernatant was disposed of. Cells were arranged on LB-Agar plates (recipe given in Supplementary Information E, Table E.3) with the appropriate antibiotics and incubated at 37°C overnight.

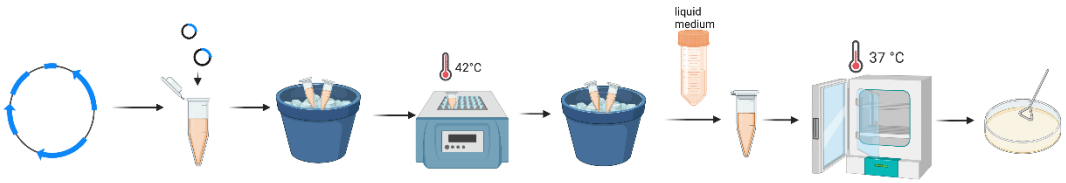

Figure 3: Overview of the heat-shock transformation protocol. Plasmid DNA was transferred into competent *E.coli* cells using the heat shock method. The transformed cells were recovered on ice and spread onto selective agar plates.

2.2. In Silico Design

To develop an appropriate system capable of detecting our target trigger sequences, suitable web-based tools were used during the design phase. In order to generate trigger sequence candidates, Primer-BLAST was used (https://www.ncbi.nlm.nih.gov/tools/primer-blast/) with optimized temperature parameters and the PCR product size set between 120-160 bp. The input sequence utilized in this process was derived from the Influenza A H1N1 genome (GenBank: CY073457.1). Next, the free energies of trigger candidates were analyzed using the web-based NUPACK software (http://www.nupack.org/), and a constraint of –25 kJ/mol was applied to select suitable designs for the next step. Trigger candidates that satisfied the energy constraint and passed BLAST analyses were further processed using the NUPACK design software to generate appropriate switch constructs. For each trigger candidate, approximately 50 switch variants were computationally designed. Following the design phase, structures containing identical sequences, stop codons, or high defect values were eliminated using a 25% defect function threshold.

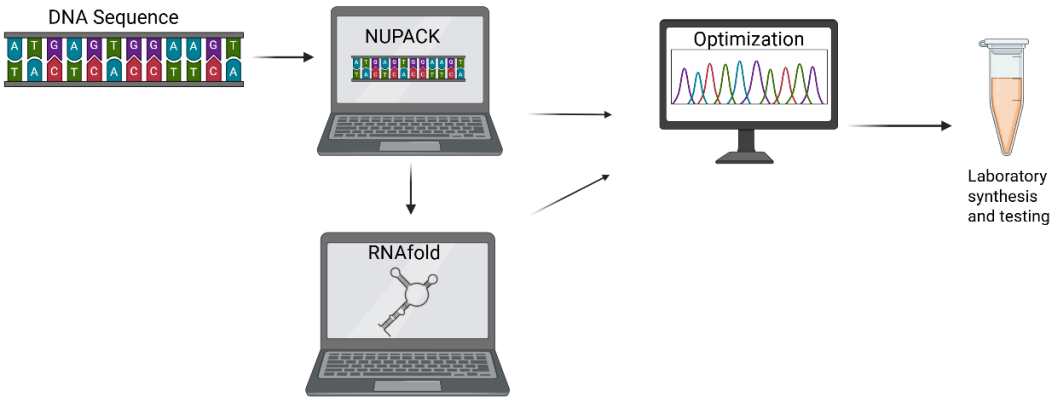

Figure 4: Computational workflow for toehold switch design and validation. The DNA sequence of interest is first analyzed using NUPACK to evaluate its secondary structure and thermodynamic stability. RNAfold is then used to further evaluate and visualize the folding of candidate toehold switch designs. Based on these computational predictions, sequence optimizations are performed to improve the performance of the switches. Finalized sequences are then synthesized and experimentally validated in the laboratory.

For each trigger targeting regions of the Influenza A H1N1 genome, the toehold domains include b*, a*, conserved domain, a and linker region as previously reported. The target-binding region includes the b* and a* domains, whereas a*, conserved domain, and a domains form the stem and loop domains. The lengths of the domains are as follows: b*-24 bp, a*-12 bp, conserved domain-28 bp (including 8 bp RBS and ATG sequences), a-12 bp, and linker region-21 bp [14].

2.3. Construction of pET-22b(+) Trigger Plasmid

Plasmids containing lacI promoter, and lacI region, namely pET-22b(+) S Protein_Trigger 2, were obtained from our lab. These plasmids contain T7 promoter, T7 terminator, and an ampicillin resistance gene. The trigger sequence, the M gene was purchased. Additionally, due to its large size, a truncated version was amplified using a specific primer pair with Q5 polymerase under recommended conditions (conditions provided in Supplementary Information E, Table E.4).

In order to construct trigger plasmid, a previously available trigger plasmid was amplified by polymerase chain reaction (PCR), with primers designed to exclude the original trigger sequence. The amplification was carried out under appropriate temperature conditions. After PCR, the amplified product was run on a 1% agarose gel containing SYBR^{TM} Safe DNA gel stain via electrophoresis at 120V for 35 minutes and the desired band was extracted and purified using the Monarch DNA Gel Extraction kit, following the manufacturer's instructions. Following the backbone amplification, the desired trigger region was similarly amplified by PCR using specific primers under optimized temperature conditions. The PCR product was then run on a 3% agarose gel at 100V for approximately 50 minutes, followed by gel extraction and purification with the same kit.

After measuring the concentration with the Thermo Scientific NanoDrop^{TM} 2000 Spectrophotometer, the resulting linear DNA fragments were assembled. Approximately 50 ng of the amplified backbone was combined

with trigger fragment at a 1:7 molar ratio using 1.33x Gibson Assembly prepared in the laboratory (reaction mix protocol given in Supplementary Information E, Table E.6). The reaction was incubated at 50°C for 1 hour. After incubation, chemical transformation was performed into *E.coli* DH5α, and the cells were spread onto LB-agar plates containing the appropriate antibiotic.

2.4. Construction of pZa-Switch Plasmid

These plasmids are constructed on the pZa backbone and contain a T7 promoter with superfolder Green Fluorescent Protein (sfGFP) reporter gene, followed by an rrnB_T1 terminator. A chloramphenicol resistance gene (CMR) is included to allow for antibiotic selection. They were obtained from our lab.

To construct the switch plasmids, candidate switch sequences generated by the web-based design tool NUPACK were first evaluated using RNAfold, another web-based software, to assess their predicted secondary structures and to ensure the absence of internal stop codons. Sequences that were found to be structurally stable and free of stop codons were selected for further analysis. For each of these selected candidates, specific primers were designed using the Primerize platform (https://primerize.stanford.edu/design_1d/) in order to enable the synthesis of the switch regions corresponding to the sequences provided by NUPACK.

Following primer design, PCR reactions were carried out to amplify the switch fragments. In parallel, PCR amplification of the plasmid backbone,

onto which the switch sequences would be inserted- was also performed under optimized conditions. The amplified switch fragments were separated by electrophoresis on a 4% agarose gel at 100V for 55 minutes, whereas the backbone was run on a 1% agarose gel at 120V for 30 minutes. After gel electrophoresis, the corresponding DNA bands were cut and purified using the Monarch DNA Gel Extraction kit.

Upon completion of the purification steps, measuring the concentration with the Thermo Scientific NanoDrop™ 2000 Spectrophotometer, the resulting linear DNA fragments were assembled. Gibson Assembly was performed by combining 50 ng of the purified backbone with the switch insert at a molar ratio of 1:9, using a prepared Gibson Assembly master mix. The reaction mixture was incubated at 50°C for 1 hour. Following assembly, chemical transformation was carried out using *E.coli* DH5α competent cells. The transformed cells were then plated on LB-agar plates containing the appropriate antibiotic for selection.

2.5. Confirmation of Constructs and Sequence Alignments

Single colonies were selected from LB-agar plates and inoculated into 3-10 mL of LB medium supplemented with the appropriate antibiotics, followed by overnight incubation at 37°C with 200rpm. The next day, cells from each culture were harvested by centrifugation at 8000 rpm for 7 minutes. After

removing the supernatant, plasmid DNA was extracted using the Monarch Plasmid Miniprep Kit according to the manufacturer's protocol.

Constructs selected for sequence verification were sent for Sanger sequencing (BM Lab). Sequence alignments were performed using either Benchling or Geneious software platforms.

For the alignments, they carried out using Benchling, Sanger sequencing results (.ab1 files) were uploaded to the platform. The multiple alignment tool was used with default parameters, applying the Multiple Alignment using Fast Fourier Transform (MAFFT) algorithm to assess whether the Sanger reads matched the intended plasmid constructs.

In the case of Geneious, the annotated plasmid file (.gb format), exported from the Bencling, and the Sanger sequencing results (.ab1 files) were imported into the software. Sequence alignment was performed to verify the correspondence between the sequencing data and the plasmid map.

2.6. Whole-Cell Sensor Test

As the first step of characterization, the switch constructs were chemically transformed into *E.coli* BL21(DE3) cells under appropriate antibiotic selection conditions. Following transformation, cells were carrying the switch plasmid were made competent using the TSS buffer protocol available in our laboratory.

For this procedure, the cells were first cultured overnight in liquid LB medium at 37°C with shaking at 200 rpm. The overnight culture was then

diluted into fresh LB medium and growth was continued at 37°C and 200 rpm until the OD_{600} reached between 0.3-0.5. Once the desired OD_{600} was achieved, the cells were placed on ice for approximately 10 minutes alongside the TSS buffer, which had been stored at -20°C until partially thawed.

Cells were then centrifuged at 3000 rpm for 10 minutes at 4°C. After centrifugation, the supernatant was discarded, and the cell pellet was gently resuspended in the chilled, liquefied TSS buffer using a pipette. These switch-competent cells were subsequently used for a second chemical transformation with the plasmid containing the corresponding trigger sequence.

As a control group, *E.coli* BL21 cells containing only the switch plasmids were used. Both the experimental (trigger+switch) and control (only switch) groups were inoculated from LB-agar plates into liquid LB medium supplemented with appropriate antibiotics and incubated overnight at 37°C and 200 rpm.

The following day, the overnight cultures were diluted 1:100 into fresh LB medium. Once the cultures reached OD_{600} of approximately 0.2-0.3, induction was carried out by adding isopropyl β-d-1-thiogalactopyranoside (IPTG) to a final concentration of 1mM. Cultures were then incubated for approximately 4 hours at 37°C with shaking at 200 rpm. For each sample, approximately 300-400 µL of culture was collected into 1.5 mL micro-centrifuge tube. and centrifuged at 14000 rpm for 2 minutes. Then the cells were resuspended in 300 µL 1x Phosphate-buffered saline (PBS) (recipe

given in Appendix E, Table E.7). After that, 200 µL resuspended samples were transferred to 96-well plates. The excitation and emission settings for the fluorescent reporter were as follows: for sfGFP, excitation was set to 485 nm and emission to 548 nm. Total fluorescence emission of the trigger plasmid carrying cells and control groups were measured by M5 Spectramax at 4 hours.

2.7. Flow Cytometry Analysis

Flow cytometry measurements were performed using the BD Accuri C6 flow cytometer. The cells used for analysis were cultured as described in the 'Whole-Cell Sensor' section. For each sample, approximately 300-400 µL of culture was collected into 1.5 mL micro-centrifuge tube. and centrifuged at 14000 rpm for 2 minutes. The supernatant was carefully removed, and the pellet was resuspended in 1 mL of 1x PBS. The suspension was then centrifuged again at 14000 rpm for approximately 2 minutes. After discarding the supernatant, the pellet was resuspended once more in 1mL of 1x PBS.

During the measurement process, the forward scatter (FSC) and side scatter (SSC) thresholds were set to 8000 in order to eliminate background. For each measurement, 100000 events were recorded, and the data were analyzed using the BD Accuri C6 Plus software.

2.8. Statistical Data Analysis

Statistical analysis and graphing of the data obtained from biosensor assays based on toehold switch constructs were performed using GraphPad Prism. Flow cytometry was used to assess the fluorescence output of cells expressing toehold switch elements in response to specific trigger sequences. All illustrations, including schematic representations of the switch-trigger mechanism and experimental workflow, were created by using BioRender.com.

CHAPTER III: RESULTS AND DISCUSSION

3.1. Cloning of Switch Plasmids

Toehold switch structures were designed to recognize conserved genomic regions of the Influenza A H1N1 virus [22, 23]. To ensure that the switch would only be activated in the presence of a specific trigger RNA sequence, each construct was placed upstream of the sfGFP reporter gene. Structural and thermodynamic evaluations were carried out using various computational tools, and sequences with the most favorable characteristics were selected. These candidate sequences were then cloned into a T7 promoter-based expression plasmid and prepared for experimental validation.

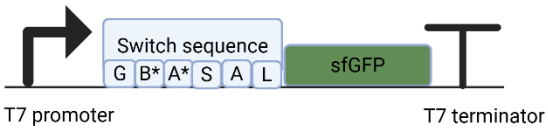

Figure 5: Schematic representation of toehold switch-based expression system. Switch sequence was cloned under the T7 promoter followed by sfGFP. Illustration is created by using BioRender.com

The design process began with computational analysis using tools like NUPACK and RNAfold, which helped evaluate the secondary structure and thermodynamic stability of each candidate toehold switch. These programs made it possible to examine important features such as the formation of stem-loop structures, how accessible the ribosome binding site was, the overall free energy of the structure, and how effectively the trigger RNA could bind to the switch region. Sequences that stayed in a closed conformation without the trigger and opened in a thermodynamically favorable way when the trigger was present were chosen for further testing.

To begin with, pZa plasmid was used as the backbone for integrating the switch sequence, which was obtained from our lab stock. The plasmid was amplified by PCR, and expected a band of approximately 2500 base pairs, as shown in figure 6.

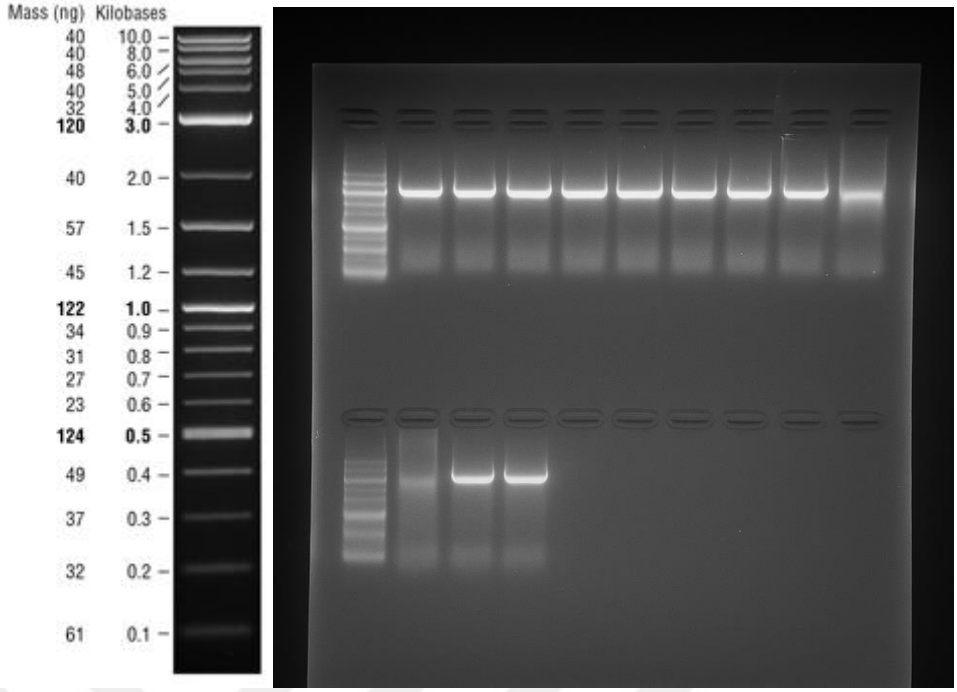

Figure 6: Agarose gel electrophoresis image showing the PCR amplification of the switch plasmid backbone. The expected band size was approximately 2500 base pairs. DNA ladder is loaded in the first column for size reference. Bright bands corresponding to the expected size confirm successful amplification of the backbone fragment.

After that, a second PCR was performed to amplify the switch region to be inserted, where we expected a band of around 120-150 base pairs, as illustrated in figure 7.

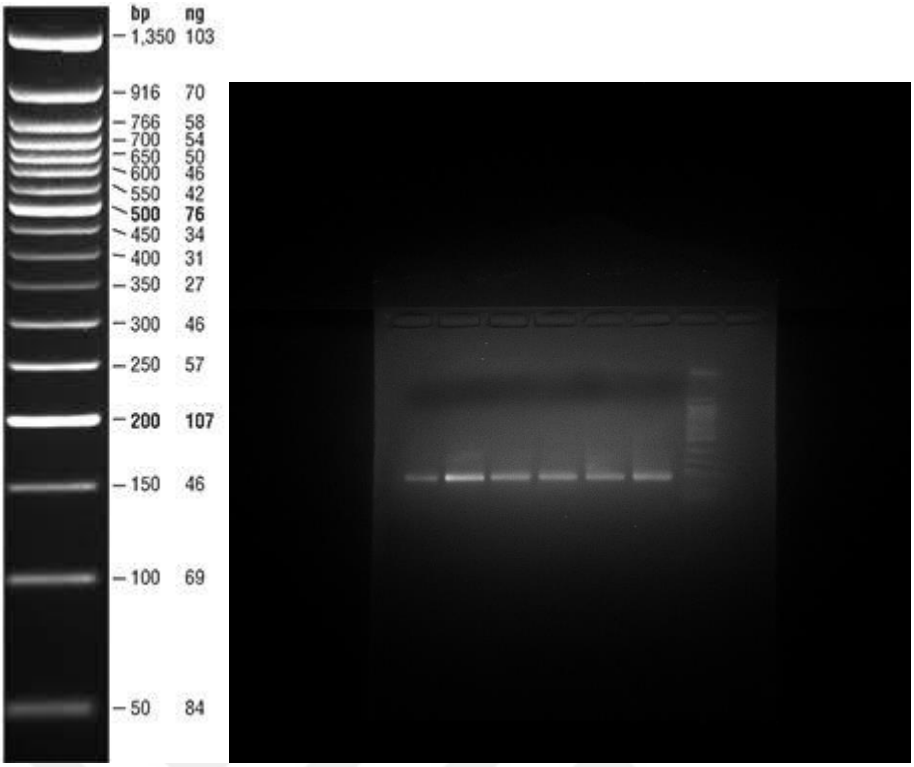

Figure 7: Agarose gel electrophoresis image of PCR-amplified switch insert sequences. Expected insert size approximately 120-150 base pairs.

After gel electrophoresis, the target bands corresponding to both the backbone and the switch insert were excised from the gel and purified. The purified fragments were then used in a Gibson Assembly reaction, set up at a 1:7 molar ratio of backbone to insert. The plasmid map of the resulting constructs are provided in appendix Figure C.

The pZa switch plasmid was transformed into *E.coli* DH5α. After the transformation, plasmid isolation is performed. Then, purified plasmid was transformed into *E.coli* BL21 (DE3) cells for protein expression. Both, strains contain the T7 promoter, allowing high-level expression of recombinant proteins when induced with IPTG.

3.2. Cloning of Trigger Plasmids

To construct the trigger plasmids, conserved regions within the genome of the Influenza A H1N1 virus were selected by analyzing sequence from NCBI's GenBank database. This approach allows for more stable and reliable design of the system. To make these regions, suitable primers were designed using the Primerize web tool, and PCR reactions were carried out under optimized temperature conditions. The resulting PCR products were run on a 4% agarose gel, and bands of approximately 200 base pairs were excised and purified as illustrated in figure 8.

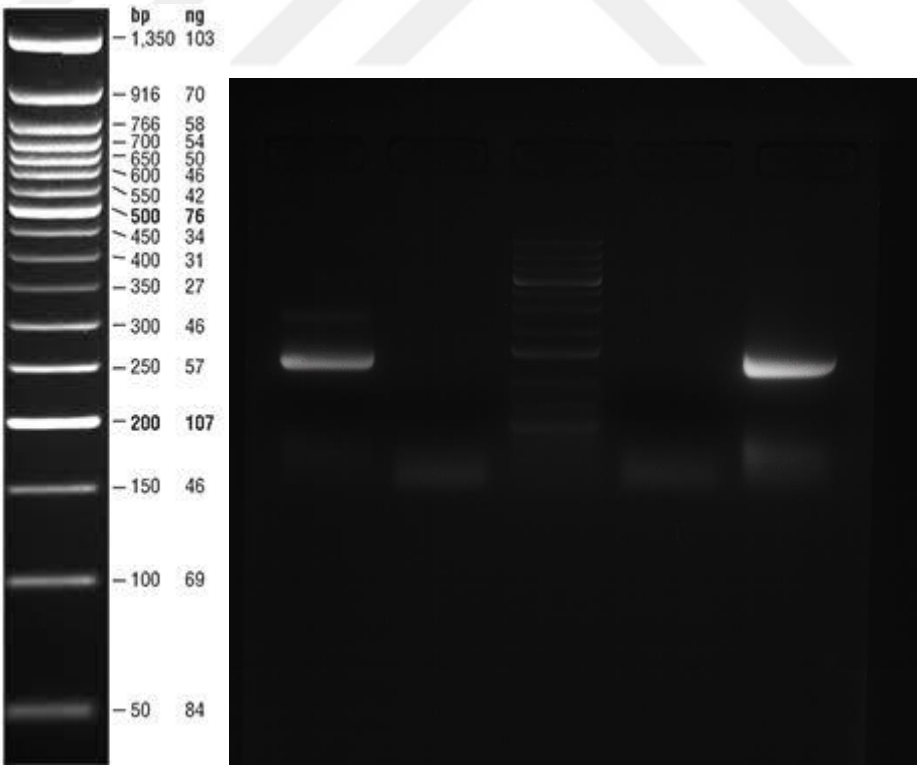

Figure 8: Agarose gel electrophoresis image of PCR-amplified trigger insert sequence. Expected insert size approximately 150–200 base pairs.

At the same time, to prepare the backbone required for the insertion of the trigger region, the pET-22b(+) plasmid, previously used in our lab, was amplified by PCR targeting specific regions of the plasmid. The amplified product was then run on a 1% agarose gel, and a band of roughly 5200 base pairs was isolated and purified, as illustrated in figure 9, for further use.

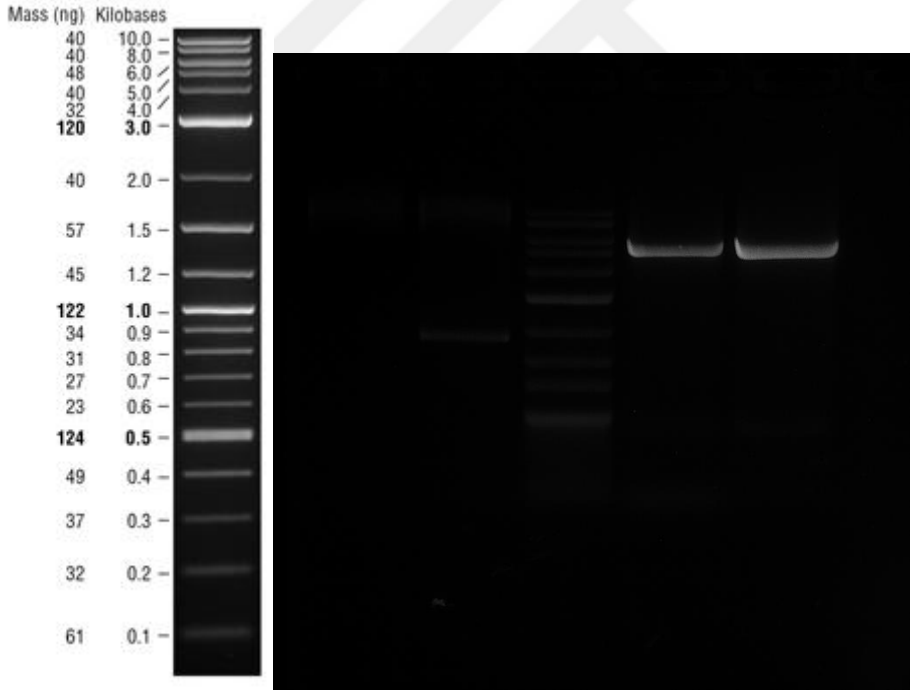

Figure 9: Agarose gel electrophoresis image of PCR-amplified trigger backbone. Expected insert size approximately 5200 base pair.

After gel electrophoresis, the backbone and trigger fragments containing the target bands were assembled using the Gibson Assembly method with a 1:7 molar ratio. Once the trigger plasmid was formed, it was introduced into *E.coli* DH5α cells. After transformation, plasmid purification was done from the cells to continue with the following steps.

3.3. Initial Functional Assessment of Trigger–Switch Constructs

Switch and trigger constructs were inserted into *E.coli* BL21 cells for functional assessment following the cloning and plasmid preparation procedures outlined in the Materials and Methods section.

First, BL21 cells were transformed using the switch plasmid. After becoming chemically competent, these cells went through transformation using the trigger plasmid. In order to determine whether the designed toehold switches remained translationally inactive in the absence of trigger RNA and became active only when the specific trigger was present, a dual-plasmid expression system was designed. After the transformation process, the resulting cell populations were used for fluorescence-based analyses.

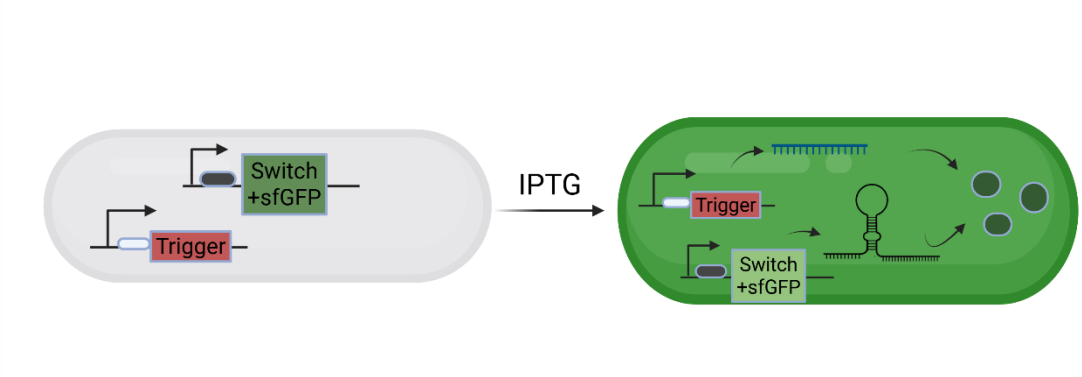

Figure 10: Schematic representation of IPTG-inducible expression of trigger and toehold switch constructs in *E.coli.* The figure shows the system designed for the expression of a toehold switch and it corresponding trigger RNA. One plasmid encodes the toehold switch regulating the translation of sfGFP, while the other carries the complementary trigger sequence. In the absence of IPTG, transcription remains inactive. Upon IPTG induction, the trigger binds to the toehold switch RNA causing the secondary structure unfold and enabling ribosome access for sfGFP translation, which leads to a fluorescent output.

During the initial stages of our experimental validation, the transformation of *E. coli* with toehold switch constructs yielded visibly green fluorescent colonies on LB agar plates supplemented with the appropriate antibiotics. This initial observation was promising, as the expression of the superfolder green fluorescent protein (sfGFP) reporter gene served as an indirect readout for the activation of our synthetic RNA switches. In theory, fluorescence should only occur when the switch construct is activated by the presence of its corresponding trigger RNA. Therefore, observing fluorescence at the colony level suggested that, at least in some contexts, the toehold design was

capable of inducing gene expression and producing functional protein in response to a regulatory input.

However, upon closer inspection, a significant issue became evident. Green fluorescence was not exclusive to colonies transformed with both the switch and the trigger plasmids; rather, colonies harboring only the toehold switch construct also displayed visible fluorescence, even in the absence of any trigger RNA. This unintended gene expression in the OFF state revealed a major limitation in the switch architecture—namely, a failure to fully repress translation in the absence of a cognate input. This phenomenon, commonly referred to as "leakiness," undermines the binary logic of synthetic biosensors and can significantly impair diagnostic specificity, especially in systems where even low-level background expression could result in false positives or misleading results.

The observed leakiness suggested that the hairpin structure within the 5′ untranslated region (5′ UTR) of the mRNA, which is designed to sequester the ribosome binding site (RBS) and start codon, was insufficiently stable. In a properly functioning toehold switch, the RBS and AUG codon are embedded within a stem-loop structure that prevents ribosomal access in the absence of a trigger. However, RNA is a dynamic molecule, and even modest instabilities in the stem-loop can lead to spontaneous breathing of the hairpin, transient exposure of the RBS, and unintended initiation of translation. The presence of such instability was consistent with the background fluorescence observed in our switch-only colonies.

To address this challenge, we undertook a targeted structural refinement approach focused on improving the thermodynamic stability of the OFF-state conformation. Specifically, we introduced two to three point mutations into the toehold domain of the construct. These mutations were not arbitrary; rather, they were selected based on structural predictions and entropy analyses performed using RNAfold and NUPACK. Our primary objective was to reinforce the stem-loop structure without compromising the trigger-binding capability of the toehold region.

A key aspect of this refinement involved increasing the guanine–cytosine (G–C) content within the second half of the toehold domain. G–C base pairs are known to form three hydrogen bonds, compared to the two hydrogen bonds in adenine–uracil (A–U) pairs, which renders G–C pairs more thermodynamically stable. By strategically placing G and C nucleotides in regions contributing to stem formation, we sought to lower the minimum free energy (MFE) of the OFF-state structure, thereby making it more resistant to spontaneous unfolding. Importantly, the introduced mutations were positioned outside of the trigger-binding interface, allowing us to preserve the complementarity and sensitivity of the switch to its cognate RNA input.

This strategy represents a broader principle in RNA synthetic biology—namely, that functional RNA devices often require precise tuning at the structural level, not just sequence matching. The challenge is to strike a delicate balance between repression and activation: the OFF-state must be stable enough to prevent basal translation, while the ON-state must be easily accessible upon trigger hybridization. Fine-tuning this balance often necessitates multiple iterations of design, modeling, and experimental testing.

In our case, the implementation of these stabilizing mutations led to a measurable decrease in background fluorescence, more clearly defined ON/OFF states, and improved reproducibility across biological replicates.

Overall, this section of our study underscores the importance of considering RNA secondary structure dynamics in the practical implementation of toehold switches. While in silico predictions provide useful starting points, experimental realities such as leakiness and inconsistent expression profiles must be addressed through iterative refinement. By reinforcing the OFF-state architecture through G–C enrichment and rationally designed mutations, we improved the functional reliability of our RNA sensor system—a crucial step toward the development of robust, field-deployable diagnostics.

After the dual transformation was completed, IPTG was added to the cultures to induce the expression of the toehold switch construct under the control of the T7 promoter [16, 24]. Following induction, the cells were incubated at 37°C with shaking at 200 rpm for 4 hours. To evaluate the system's output, both microplate-based fluorescence measurement and flow cytometry were used.

For bulk fluorescence analysis, OD_{600} and fluorescence values (excitation at 485 nm, emission at 538 nm) were measured using an M5 microplate reader. Each measurement was carried out in three replicates. To correct for differences in cell growth, fluorescence intensity values were normalized to the optical density at 600 nm, and the resulting RFU/ OD_{600} ratios were used to compare different conditions. This analysis provided preliminary insights

into general expression patterns and helped distinguish between functional and non-functional trigger-switch pairs.

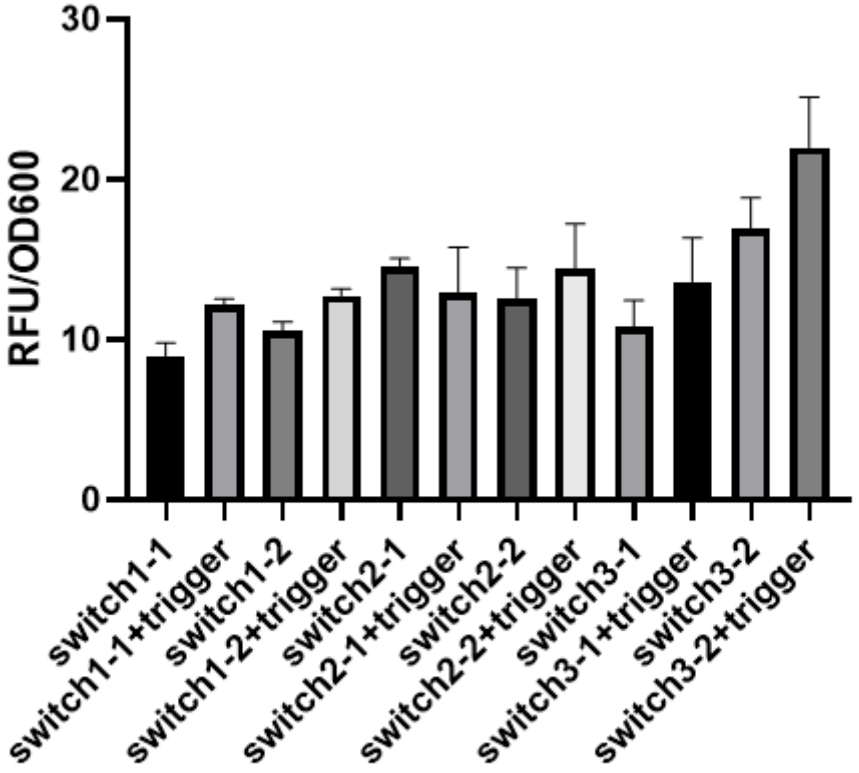

Figure 11: Microplate reader results for fluorescence output of various toehold switch constructs with and without trigger RNA.

To better evaluate the system at the single-cell level, flow cytometry was used. This method helped show the differences in sfGFP expression between indiviual cells and made it easier to see if there was real activation by the

trigger or just background signal. In this part, only switch and switch+trigger groups were tested.

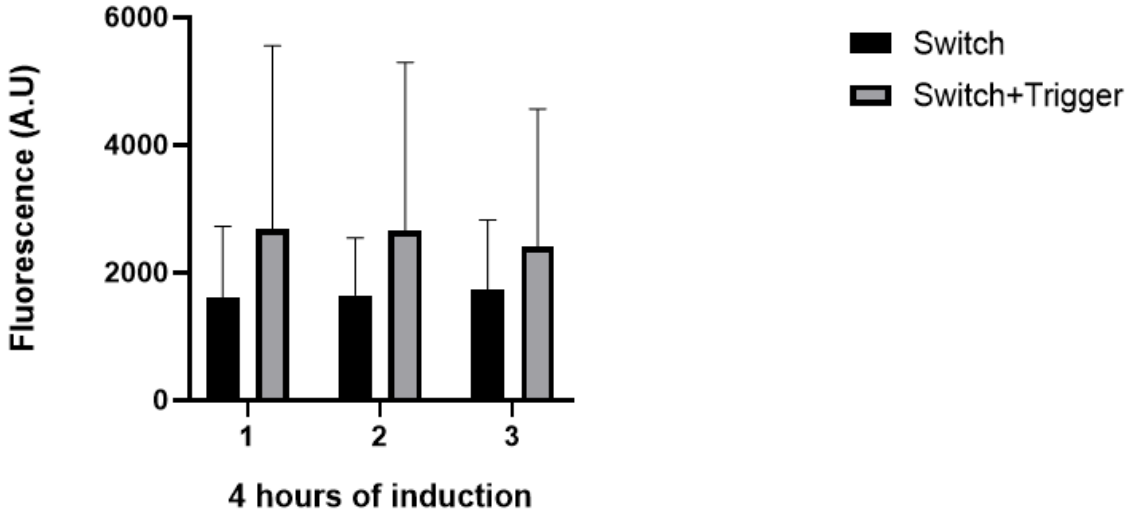

Figure 12: Flow cytometer results for fluorescence analysis of switch and switch+trigger systems after 4 hours of IPTG induction.

The cells were induced with IPTG and incubated at 37°C for 4 hours. No significant difference was observed between the switch-only and switch+trigger groups.

These results suggest that the designed switch constructs were not sufficiently activated under the tested conditions. Based on these experimental results, it became clear that the current switch and trigger designs require further optimization. Improvements in sequence selection,

structural stability, or expression conditions might be necessary to achieve stronger and more reliable activation in response to the target trigger RNA.

3.4. Optimization of Toehold Switch Constructs

In our earlier experiments, we noticed that some of the toehold switch constructs did not perform as expected. While a few designs showed good control—turning the signal ON only when the trigger RNA was present—others showed green fluorescence even without the trigger. This suggested that some switches were not properly repressed in their OFF state, meaning they allowed gene expression when they were not supposed to. To understand why this happened, we went back and looked more closely at the structures of these problematic designs.

To do this, we used two online tools: RNAfold and NUPACK. Both tools are commonly used to predict how an RNA sequence will fold into its secondary structure. They help us see which parts of the RNA are likely to form base pairs and which parts stay single-stranded. These predictions are important because the shape of the RNA affects how it behaves—especially in toehold switches, which rely on folding and unfolding to control translation. [26, 27].

One key feature we focused on was the toehold binding region—the part of the switch that is supposed to bind the trigger RNA. For the switch to work properly, this region needs to be unpaired and easy to reach, so the trigger can attach and open up the hairpin structure. If this region is involved in

internal base-pairing (for example, if it folds onto itself), the trigger cannot easily bind, and the switch might not respond well. So, we paid close attention to how many unpaired bases there were in this region in each design.

RNAfold allowed us to view predicted structures using dot-bracket notation and base pairing diagrams. We also looked at positional entropy plots, which show how stable or flexible different parts of the RNA are. In well-performing designs, the toehold region had low base pairing and moderate entropy—meaning it was exposed enough to interact with the trigger but not so unstable that it folded into the wrong shapes. In contrast, poor-performing switches often had the toehold region folded into stem structures, making it harder for the trigger to access.

NUPACK gave us a second opinion and allowed us to compare how often certain regions were open or closed across possible structures. It also provided something called the ensemble defect, which tells us how far the actual folding of the RNA is from the ideal design. Lower defect values suggest that most of the RNA molecules fold the way we want them to. We found that good designs had lower ensemble defect scores and better accessibility in the toehold region.

To help visualize all of this, we included diagrams generated from RNAfold and NUPACK in our figures. These show examples of both strong and weak switch designs. In the better switches, the ribosome binding site (RBS) and start codon were hidden in a stable stem-loop, while the toehold region was mostly unstructured. In the weaker ones, the toehold sequence was tangled

with other parts of the RNA, or the structure was too loose, leading to unintended expression.

Thanks to these visual and numerical analyses, we gained a better understanding of why some switches didn't work well. Based on this, we made design changes such as increasing the number of G and C bases to stabilize stems, moving the location of loops, or adjusting the spacing between regions to avoid unwanted interactions. These small changes were guided by what we saw in the structure predictions and helped improve performance in later versions.

In conclusion, this structural analysis showed that how an RNA folds plays a major role in whether a toehold switch works correctly. Especially in the toehold region, having unpaired, accessible bases is very important. Using tools like RNAfold and NUPACK early in the design process can save time by predicting problems before lab experiments. By combining these tools with experimental testing, we can make more reliable and effective synthetic RNA sensors [28, 29].

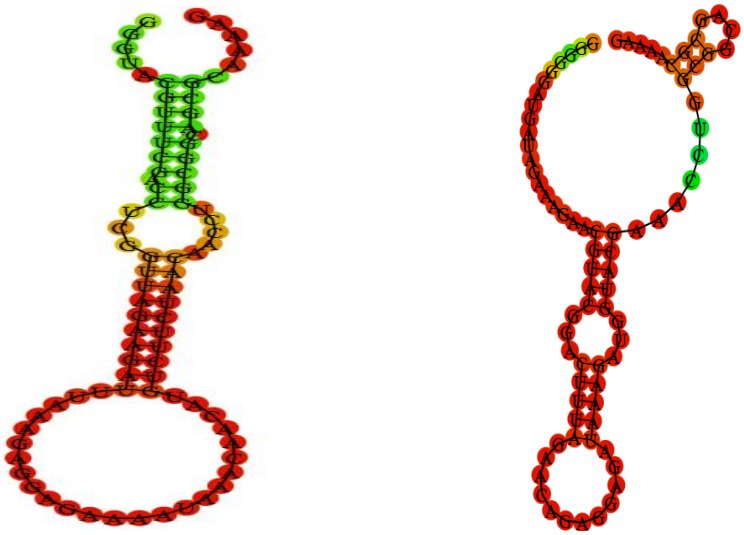

Figure 13: Secondary structure predictions were made for two different toehold switch designs using RNAfold web-tool. In the structure on the left, the toehold domain is highly closed and the 5’ end is tightly connected by base pairing. This structure may make it difficult to access the RBS and make it difficult to activate by the trigger RNA. The structure on the right has a more open conformation, with the 5’ end largely exposed and accessible. This openness may facilitate trigger recognition of the site and make translation initiation more efficient. The difference between these two structures suggest that the openness of the toehold domain has a significant impact on the responsiveness of synthetic RNA editors [11].

3.5. Thermodynamic Evaluation and Redesign of Toehold Switches

In RNA-based systems like toehold switches, RNA secondary structure plays a critical role in determining whether the switch functions correctly. One of the most important factors used to evaluate RNA structure is the Gibbs free energy, also known as ΔG. This value gives us an idea of how stable an RNA molecule's folded shape is. In simple terms, a more negative ΔG means that the structure is more stable, while a less negative (or closer to zero) ΔG means that the RNA structure is less stable or more open.

When designing a toehold switch, our goal is to create an RNA molecule that stays "closed" in the absence of the trigger and only "opens" when the trigger RNA is present. In the OFF state, the switch needs to fold into a structure that hides important parts like the ribosome binding site (RBS) and start codon, so that the ribosome cannot start translation. A stable structure helps achieve this goal by keeping those regions safely paired in a stem-loop formation. Here, a strong (more negative) ΔG supports the OFF state by ensuring the RNA does not easily unfold or expose the RBS unintentionally.

However, this situation becomes tricky if the structure is too stable. If ΔG is very negative, the switch may form a structure that is too tight or rigid. In such cases, even when the correct trigger RNA is present, it may not be able to bind easily and open the structure. As a result, the switch might stay OFF even though it should turn ON. This leads to poor responsiveness and weak signal detection.

On the other hand, if ΔG is not negative enough—for example, if it is closer to 0—the structure may be too loose. This means that the RBS or start codon may become accidentally exposed, even without a trigger RNA. When that happens, the ribosome may begin translation even though the switch is supposed to be OFF. This causes background expression or leakiness, which is a common problem in synthetic RNA designs. Such leakiness makes it hard to distinguish between the presence and absence of the trigger, reducing the accuracy and reliability of the system.

Because of these issues, it is important to find a balance. A well-functioning toehold switch needs to be stable enough to block unwanted gene expression in the OFF state, but not so stable that it resists activation by the trigger. From past studies and practical experience, it has been observed that ΔG values between -12 and -20 kcal/mol often give the best results. In this range, the RNA forms a stable structure that stays OFF under normal conditions, but still allows enough flexibility for the trigger to bind and open the switch when needed.

It’s also important to remember that ΔG is not the only factor affecting performance. Other things, like the position of unpaired bases, the GC content, and the specific folding pattern, also matter. But ΔG gives a quick and useful way to compare different switch designs during the early design process. Tools like RNAfold and NUPACK calculate ΔG values automatically when predicting RNA structures, making them very helpful for screening large numbers of candidate sequences.

In this study, we used ΔG values as one of the main criteria to evaluate and optimize our toehold switch designs. When we saw ΔG values that were too negative (stronger than -25 kcal/mol), we tried to slightly weaken the stem structure by introducing mutations that reduced base-pairing. When the values were too close to 0 (e.g., around -8 kcal/mol), we added more GC pairs or redesigned the sequence to create a stronger stem-loop. By keeping ΔG values within the target range, we improved the balance between stability and responsiveness.

In conclusion, ΔG is a key design parameter in RNA-based systems. It provides important information about whether a toehold switch will stay OFF when it should, and whether it will activate properly when the trigger is present. Maintaining ΔG in an optimal range helps reduce background expression and ensures better ON/OFF control, which is critical for applications like diagnostics or gene regulation in synthetic biology. [15, 26, 30, 31].

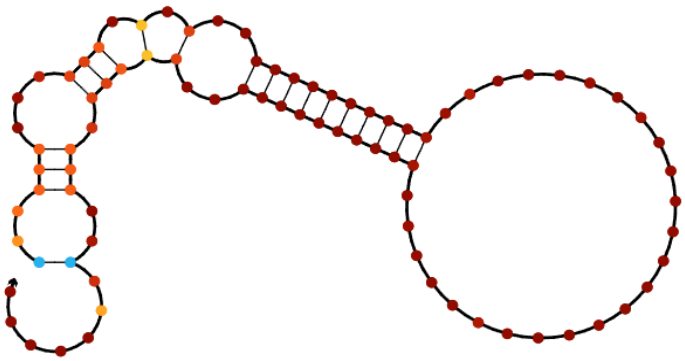

Free energy of the secondary structure: -20.39 kcal/mol

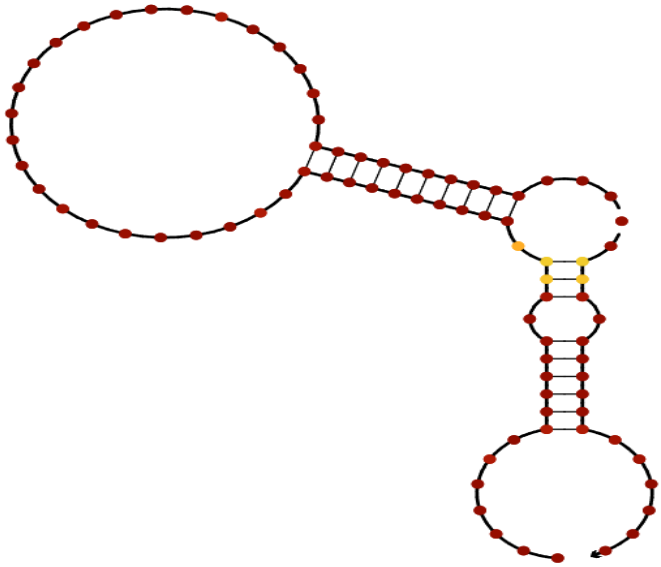

Free energy of the secondary structure: -27.13 kcal/mol

Figure 14: The minimum free energy (MFE) values of two RNA secondary structures are compared. With a free energy of -20.39 kcal/mol, the first structure (top) has a comparatively less stable conformation. Because of its relatively high energy, the structure may unfold more easily when the trigger RNA binds. The second structure (bottom) has a more compact, stable fold

and a lower free energy of −27.13 kcal/mol. It may be more difficult to unfold in response to the trigger because of the structure's increased rigidity and stiffness caused by the long hairpin regions and the absence of unpaired bases. Overall, the first structure is more prone to conformational changes and might be more vulnerable to trigger-mediated activation, whereas the second structure is thermodynamically more stable.

3.6. Comparison of Switch Positional Entropy Profiles

To better understand why some toehold switch designs worked well and others did not, we looked at the positional entropy values of each RNA structure. These values were calculated using the RNAfold web tool which provides not only the predicted minimum free energy structure, but also information about how flexible or uncertain each position in the RNA is. This analysis helped us compare different switch designs and see where they might be too rigid or too loose. [32]. In simple terms, positional entropy tells us how much variation there is in base pairing at each nucleotide. If a position has low entropy, it means that this base is almost always paired in the same way in most of the predicted structures. This region is therefore very stable and has a fixed structure. On the other hand, if the entropy is high, it means that the base can form many different pairings, or stay unpaired. This makes the region more flexible or dynamic.

Both stability and flexibility are important in RNA structure, but their placement matters. For example, in areas like the stem of the switch, which is supposed to hold the ribosome binding site (RBS) and start codon hidden, we

want low entropy. This part of the RNA needs to stay tightly closed in the OFF state, so that no translation occurs unless the trigger RNA is present.

However, in regions near the RBS or the start codon, or in the toehold region where the trigger is expected to bind, having some entropy—meaning some flexibility—is actually useful. If these areas are too rigid, the trigger RNA may not be able to bind effectively, or the ribosome may not be able to access the start codon once the switch opens. In this case, the switch might fail to turn ON even when the trigger is present. On the other hand, if these regions are too flexible, the RBS might become accidentally exposed even without a trigger, leading to background expression or leakiness.

By comparing the entropy plots of our different switch designs, we noticed clear differences. Some switches showed moderate entropy in the right places—like just before the RBS or in the toehold region. These switches tended to perform better in experiments. Others showed very high entropy throughout, including in the stem region. These designs were more likely to have uncontrolled expression in the OFF state. We also saw designs that were too stable, with almost no entropy anywhere. These were harder to activate with the trigger.

In Figure 15, we show the positional entropy graph of two example switch designs. The better-performing switch has low entropy in the stem (keeping it shut), but slightly higher entropy near the toehold and start codon. This allows the trigger to bind and the ribosome to start translation when needed. The weaker switch, however, has high entropy even in the stem region, which may explain why it allowed gene expression even without the trigger.

Overall, entropy analysis gives us a useful way to evaluate RNA designs beyond just looking at their predicted structure or ΔG value. It helps us understand how consistent or variable each part of the RNA is across the whole folding ensemble. This is especially important for synthetic systems like toehold switches, where the function depends on precise folding behavior.

In conclusion, looking at positional entropy helps explain why some toehold switches respond better to their trigger RNAs than others. A good design needs the right balance: stable enough to stay OFF when needed, but flexible enough to switch ON when the trigger is present. Using tools like RNAfold to study entropy can make the design process more informed, reducing guesswork and improving experimental success [16, 33, 34, 35, 36].

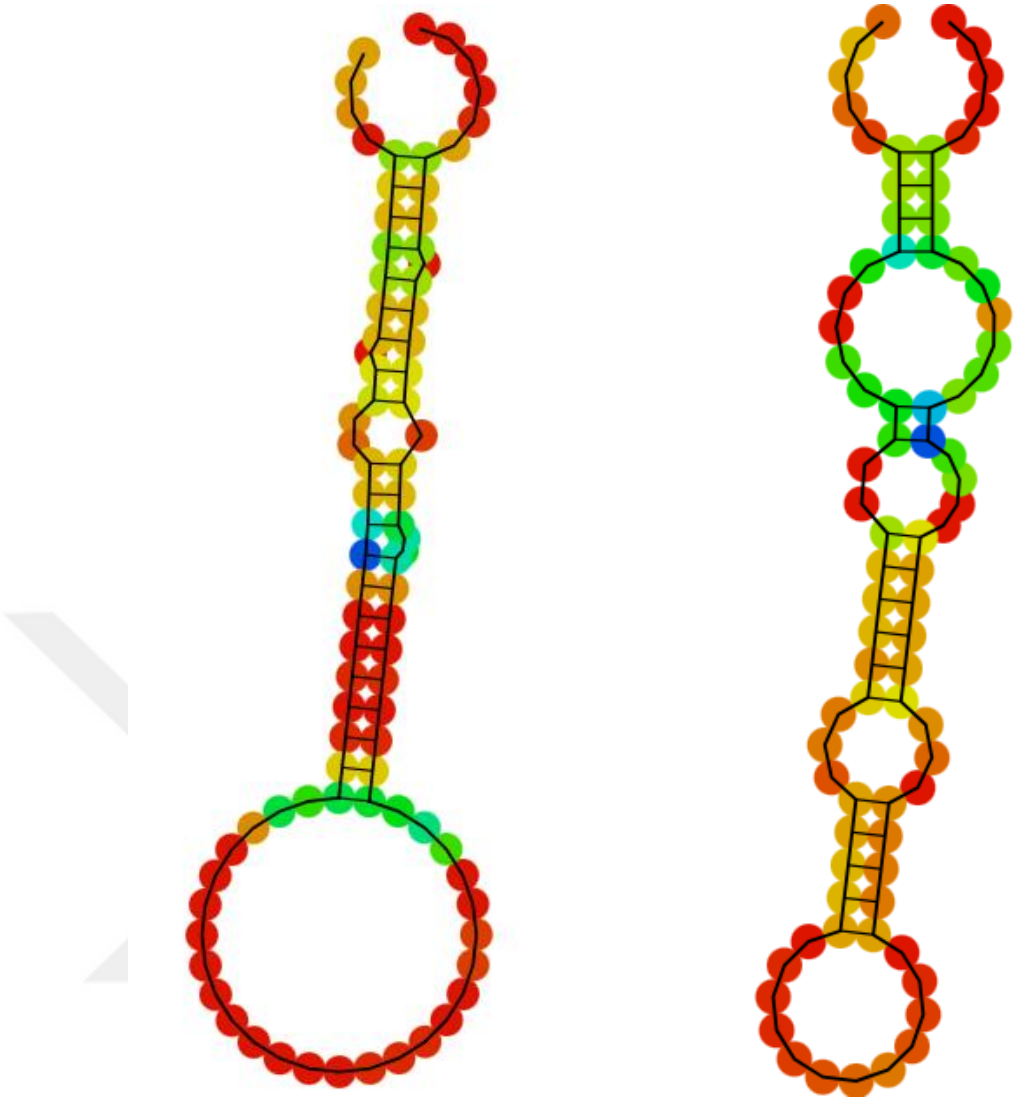

Figure 15: Comparison of secondary structure colored according to positional entropy reflecting the variability of base pairing in two different toehold switch designs. The first structure (left) shows orange-red tones throughout most of the stem region, including the hairpin structure, and especially the RBS region, indicating low entropy and stable base pairing. The second structure (right) shows more widespread entropy, with green, yellow, and blue hues, including the RBS region. This increased structural flexibility facilitates access to functional domains such as the trigger RNA binding site and the RBS. These structural differences help inform how positional entropy

profiles can be used to predict the responsiveness and leakage potential of synthetic riboregulators.

3.7. Experimental Validation of Structurally Optimized Switches

Following the structural evaluation and entropy-based optimizations of the toehold switch designs in the previous sections, experimental validation was carried out to evaluate the translation efficiency and functional performance of the obtained structures. At this stage, the aim was to determine whether the structural improvements made in line with secondary structure and positional entropy profiles translated into better gene expression.

To achieve this, representative switch structures were selected from both pre- and post- optimization stages. Pre-optimization designs were chosen based on sequence properties and predicted structural conformations. In contrast, final designs were refined using positional entropy data obtained from RNAfold analysis. Regions with very high entropy near key functional motifs, such as the RBS and start codon, were linked to reduced accessibility, which can result in poor translation efficiency. Structural adjustments were therefore introduced to improve local configurations around these regions while preserving the overall integrity of the switch.

Each construct was cloned into a standard plasmid backbone under the control of the T7 promoter and subjected to experiments. Experiments were performed in the presence and absence of target trigger RNA.

It was revealed that there was a performance difference, although not very significant, between the unoptimized and optimized structures. The initial designs generally exhibited lower and less stable expression levels, and the fold-change values varied considerably between test repetitions. Moreover, some of these unoptimized switches paradoxically showed higher reporter activity in the absence of the trigger compared to when the trigger was present, indicating an issue with structural leakiness and insufficient regulation [12, 16]. On the other hand, the optimized switch structures showed more consistent and stable responses across independent replicates, as shown in figure 16. They not only maintained their fold-change values across tests but also exhibited a clearer distinctions between triggered and untriggered states, suggesting improved control over gene expression and enhanced structural integrity.

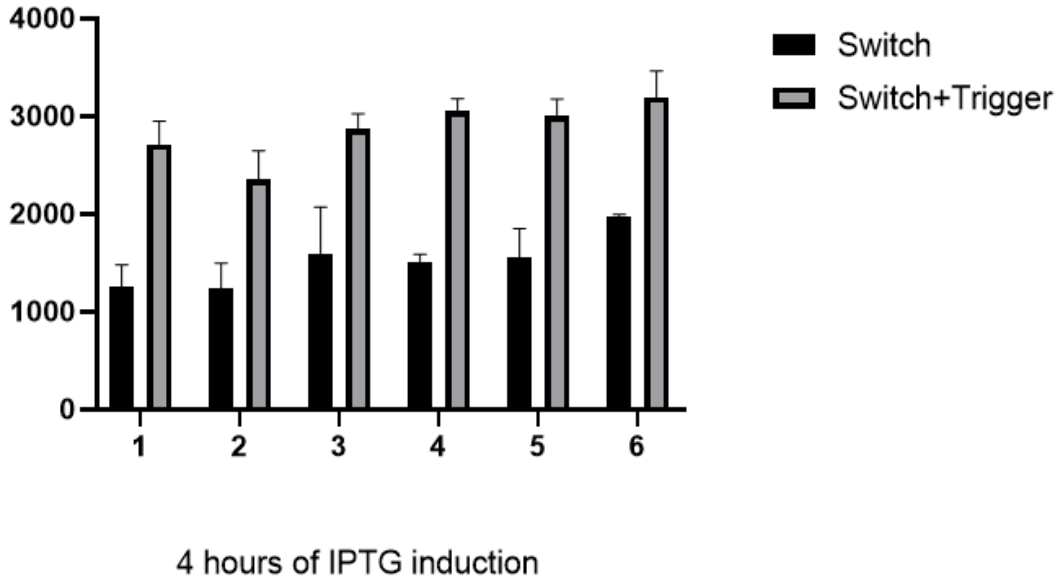

Figure 16: Flow cytometer results for optimized switches. With consistent and repeatable expression levels across triplicates, optimized switch designs

showed noticeably better ON/OFF ratios. Previously, however, non-optimized designs showed lower fold-change and higher background expression. These findings validate the significance of entropy-guided optimization techniques by confirming that structural refinements improved the dynamic range and stability of switch behavior.

CHAPTER IV: CONCLUSION

In this study, a synthetic toehold switch-based RNA sensor system was designed and experimentally validated for the detection of Influenza A H1N1 viral sequences. The goal was to explore the potential of programmable RNA regulators in a cell-free context for rapid, portable, and specific viral diagnostics. By integrating sequence-based design principles with structural modeling and entropy analysis, we sought to create functional toehold switches capable of controlling gene expression in response to defined RNA inputs.

Toehold switches offer several distinct advantages compared to traditional detection platforms. Their programmability, modularity, and compatibility with cell-free systems position them as promising candidates for next-generation diagnostics. However, their function is critically dependent on the conformational landscape of the RNA molecule, which governs accessibility, stability, and translational activation. Our work provides an in-depth analysis of how structural properties—particularly local folding and positional entropy near regulatory motifs such as the ribosome binding site (RBS) and start codon—affect the overall performance of synthetic switches.

The rational design process began with the selection of conserved H1N1 viral RNA segments and proceeded with the generation of candidate switch constructs based on established sequence heuristics. These designs were then evaluated using RNAfold and NUPACK tools, which enabled thermodynamic profiling and entropy visualization. High entropy zones,

particularly those surrounding the trigger-binding domain and translation initiation elements, were identified as potential barriers to effective gene expression. Such regions are prone to undesirable folding events that could sequester critical sites, leading to reduced dynamic range and increased background expression.

By targeting these high-entropy regions for optimization, we implemented a strategy rooted in structural refinement. The re-design phase included alterations to stem-loop stability, trigger-hairpin interactions, and loop geometry, guided by entropy plots and minimum free energy (MFE) models. The goal was to increase ribosomal access while preserving switch-trigger specificity. While these adjustments did not result in dramatic increases in fold-change values, they consistently produced more reproducible ON/OFF behavior and reduced leakiness across biological replicates—an important characteristic for diagnostic reliability.

Despite moderate improvements, several performance limitations remained. For instance, not all constructs responded to trigger RNA with the desired binary behavior. This may reflect intrinsic design constraints or limitations in cell-free system components such as magnesium ion concentration, energy regeneration pathways, or RNase contamination. Additionally, the dynamic range of activation—defined as the fold-difference between ON and OFF states—was bounded, suggesting that even structurally optimized switches can plateau in performance due to system-level bottlenecks. These findings are consistent with previous reports in the literature, which highlight the difficulty of achieving sharp, digital-like behavior in RNA-based devices without auxiliary amplification or signal processing components.

One of the core takeaways from this study is the confirmation that local RNA structure, especially near functional elements, plays a pivotal role in determining toehold switch performance. Even subtle differences in folding energy or entropy distribution can lead to substantial changes in translational output. This aligns with a broader body of work in the field of synthetic biology that emphasizes the need to treat RNA as a dynamic, context-sensitive biomolecule rather than a static scaffold. The use of entropy-guided refinement, while still an emerging methodology, shows promise in informing more predictable and tunable designs.

Moving forward, several avenues for improvement are apparent. First, coupling toehold switches with isothermal amplification techniques, such as NASBA or RPA, could significantly enhance sensitivity and expand detection limits. Second, encapsulating the system into lyophilized, paper-based formats would support field-deployable diagnostic devices, especially in resource-limited settings. Prior studies from the Green Lab and others have demonstrated the feasibility of such integration, but further engineering is needed to stabilize RNA reagents and improve long-term storage.

Moreover, advances in machine learning and generative RNA modeling now offer exciting prospects for automated switch design. By training models on large datasets of switch performance and structural features, it may be possible to predict optimal designs with higher accuracy than human-guided heuristics alone. Integrating these computational approaches with empirical screening pipelines could accelerate development cycles and lower costs.

From a broader perspective, this study contributes to the growing field of synthetic RNA biology, where tools like toehold switches, riboregulators, and CRISPR-based sensors are transforming how we detect and respond to biological signals. In particular, our findings underscore the importance of merging in silico design with in vitro testing—a principle that will be increasingly vital as the field moves toward more complex regulatory circuits and multi-input logic devices.

The use of cell-free systems also presents a paradigm shift in diagnostics and molecular programming. By decoupling gene expression from living cells, cell-free platforms eliminate many regulatory and safety barriers, enabling rapid prototyping and faster deployment. Their tunability and ease of use make them ideal for educational tools, environmental monitoring, and point-of-care testing. However, this potential will only be realized through continued innovation in system stability, scalability, and standardization.

In conclusion, while the improvements observed in our work were modest, they were consistent, reproducible, and supported by mechanistic insights. The application of entropy-guided structural refinement represents a novel and effective strategy to fine-tune RNA-based regulatory elements. The results reinforce the notion that successful biosensor development must consider both sequence and structure, and that even subtle changes in folding can lead to meaningful functional outcomes.

Future research should aim to refine this methodology further, perhaps by incorporating real-time folding dynamics, integrating synthetic RNA libraries for high-throughput screening, or testing switch performance under clinically

relevant conditions. Ultimately, the lessons learned from this study pave the way for more robust, scalable, and accessible diagnostic platforms, contributing not only to pandemic preparedness but also to the foundational understanding of synthetic RNA regulation.

BIBLIOGRAPHY

[1] F. Krammer *et al.*, "Influenza," *Nat. Rev. Dis. Primer*, vol. 4, no. 1, June 2018, doi: 10.1038/s41572-018-0002-y.

[2] R. J. Garten *et al.*, "Antigenic and Genetic Characteristics of Swine-Origin 2009 A(H1N1) Influenza Viruses Circulating in Humans," *Science*, vol. 325, no. 5937, pp. 197–201, July 2009, doi: 10.1126/science.1176225.

[3] "Emergence of a Novel Swine-Origin Influenza A (H1N1) Virus in Humans," *N. Engl. J. Med.*, vol. 360, no. 25, pp. 2605–2615, June 2009, doi: 10.1056/nejmoa0903810.

[4] J. K. Taubenberger and D. M. Morens, "1918 Influenza: the Mother of All Pandemics," 1918.

[5] S. M. Zimmer and D. S. Burke, "Historical Perspective — Emergence of Influenza A (H1N1) Viruses," *N. Engl. J. Med.*, vol. 361, no. 3, pp. 279–285, July 2009, doi: 10.1056/nejmra0904322.

[6] S. J. Sullivan, R. M. Jacobson, W. R. Dowdle, and G. A. Poland, "2009 H1N1 Influenza," *Mayo Clin. Proc.*, vol. 85, no. 1, pp. 64–76, Jan. 2010, doi: 10.4065/mcp.2009.0588.

[7] S. Echevarría-Zuno *et al.*, "Infection and death from influenza A H1N1 virus in Mexico: a retrospective analysis," *The Lancet*, vol. 374, no. 9707, pp. 2072–2079, Dec. 2009, doi: 10.1016/s0140-6736(09)61638-x.

[8] R. P. Chauhan and M. L. Gordon, "An overview of influenza A virus genes, protein functions, and replication cycle highlighting important updates," *Virus Genes*, vol. 58, no. 4, pp. 255–269, Aug. 2022, doi: 10.1007/s11262-022-01904-w.

[9] Q. Qian *et al.*, "Advances in Diagnostic Techniques for Influenza Virus Infection: A Comprehensive Review," *Trop. Med. Infect. Dis.*, vol. 10, no. 6, p. 152, May 2025, doi: 10.3390/tropicalmed10060152.

[10] P. L. Voyvodic and J. Bonnet, "Cell-free biosensors for biomedical applications," *Curr. Opin. Biomed. Eng.*, vol. 13, pp. 9–15, Mar. 2020, doi: 10.1016/j.cobme.2019.08.005.

[11] A. A. Green, P. A. Silver, J. J. Collins, and P. Yin, "Toehold Switches: De-Novo-Designed Regulators of Gene Expression," *Cell*, vol. 159, no. 4, pp. 925–939, Nov. 2014, doi: 10.1016/j.cell.2014.10.002.

[12] I. C. Koksaldi, D. Park, A. Atilla, H. Kang, J. Kim, and U. O. S. Seker, "RNA-Based Sensor Systems for Affordable Diagnostics in the Age of Pandemics," *ACS Synth. Biol.*, vol. 13, no. 4, pp. 1026–1037, Apr. 2024, doi: 10.1021/acssynbio.3c00698.

[13] K. Pardee *et al.*, "Rapid, Low-Cost Detection of Zika Virus Using Programmable Biomolecular Components," *Cell*, vol. 165, no. 5, pp. 1255–1266, May 2016, doi: 10.1016/j.cell.2016.04.059.

[14] M. K. Takahashi *et al.*, "A low-cost paper-based synthetic biology platform for analyzing gut microbiota and host biomarkers," *Nat. Commun.*, vol. 9, no. 1, p. 3347, Aug. 2018, doi: 10.1038/s41467-018-05864-4.

[15] J. N. Zadeh *et al.*, "NUPACK: Analysis and design of nucleic acid systems," *J. Comput. Chem.*, vol. 32, no. 1, pp. 170–173, Jan. 2011, doi: 10.1002/jcc.21596.

[16] R. Lorenz *et al.*, "ViennaRNA Package 2.0," *Algorithms Mol. Biol.*, vol. 6, no. 1, p. 26, Nov. 2011, doi: 10.1186/1748-7188-6-26.

[17] İ. Ç. Köksaldı *et al.*, "SARS-CoV-2 Detection with De Novo-Designed Synthetic Riboregulators," *Anal. Chem.*, vol. 93, no. 28, pp. 9719–9727, July 2021, doi: 10.1021/acs.analchem.1c00886.

[18] A. Geraldi, N. N. T. Puspaningsih, and F. Khairunnisa, "Update on the Development of Toehold Switch-Based Approach for Molecular Diagnostic Tests of COVID-19," *J. Nucleic Acids*, vol. 2022, p. 7130061, May 2022, doi: 10.1155/2022/7130061.

[19] K. Morey, T. Thomas-Fenderson, A. Watson, J. Sebesta, C. Peebles, and C. Gentry-Weeks, "Toehold switch plus signal amplification enables rapid detection," *Biotechnol. J.*, vol. 18, no. 12, p. 2200607, 2023, doi: 10.1002/biot.202200607.

[20] C. E. Copeland, A. Langlois, J. Kim, and Y.-C. Kwon, "The cell-free system: A new apparatus for affordable, sensitive, and portable healthcare," *Biochem. Eng. J.*, vol. 175, p. 108124, Nov. 2021, doi: 10.1016/j.bej.2021.108124.

[21] D. Jeong *et al.*, "Cell-Free Synthetic Biology Platform for Engineering Synthetic Biological Circuits and Systems," *Methods Protoc.*, vol. 2, no. 2, p. 39, May 2019, doi: 10.3390/mps2020039.

[22] K. Pardee *et al.*, "Portable, On-Demand Biomolecular Manufacturing," *Cell*, vol. 167, no. 1, pp. 248-259.e12, Sept. 2016, doi: 10.1016/j.cell.2016.09.013.

[23] A. T. Heiny *et al.*, "Evolutionarily Conserved Protein Sequences of Influenza A Viruses, Avian and Human, as Vaccine Targets," *PLoS ONE*, vol. 2, no. 11, p. e1190, Nov. 2007, doi: 10.1371/journal.pone.0001190.

[24] Q. Lin, X. Ji, F. Wu, and L. Ma, “Conserved Sequence Analysis of Influenza A Virus HA Segment and Its Application in Rapid Typing,” *Diagnostics*, vol. 11, no. 8, p. 1328, July 2021, doi: 10.3390/diagnostics11081328.

[25] A. D. Silverman, A. S. Karim, and M. C. Jewett, “Cell-free gene expression: an expanded repertoire of applications,” *Nat. Rev. Genet.*, vol. 21, no. 3, pp. 151–170, Mar. 2020, doi: 10.1038/s41576-019-0186-3.

[26] K. Sato, M. Akiyama, and Y. Sakakibara, “RNA secondary structure prediction using deep learning with thermodynamic integration,” *Nat. Commun.*, vol. 12, no. 1, p. 941, Feb. 2021, doi: 10.1038/s41467-021-21194-4.

[27] D. H. Mathews, J. Sabina, M. Zuker, and D. H. Turner, “Expanded sequence dependence of thermodynamic parameters improves prediction of RNA secondary structure,” *J. Mol. Biol.*, vol. 288, no. 5, pp. 911–940, May 1999, doi: 10.1006/jmbi.1999.2700.

[28] S.-J. Kim, M. Leong, M. B. Amrofell, Y. J. Lee, and T. S. Moon, “Modulating Responses of Toehold Switches by an Inhibitory Hairpin,” *ACS Synth. Biol.*, vol. 8, no. 3, pp. 601–605, Mar. 2019, doi: 10.1021/acssynbio.8b00488.

[29] T. Hoang Trung Chau, D. Hoang Anh Mai, D. Ngoc Pham, H. Thi Quynh Le, and E. Yeol Lee, “Developments of Riboswitches and Toehold Switches for Molecular Detection—Biosensing and Molecular Diagnostics,” *Int. J. Mol. Sci.*, vol. 21, no. 9, p. 3192, Apr. 2020, doi: 10.3390/ijms21093192.

[30] N. M. Angenent-Mari, A. S. Garruss, L. R. Soenksen, G. Church, and J. J. Collins, “A deep learning approach to programmable RNA switches,” *Nat. Commun.*, vol. 11, no. 1, p. 5057, Oct. 2020, doi: 10.1038/s41467-020-18677-1.

[31] “Accurate SHAPE-directed RNA structure determination.” Accessed: July 09, 2025. [Online]. Available: https://www.pnas.org/doi/epdf/10.1073/pnas.0806929106

[32] A. R. Gruber, R. Lorenz, S. H. Bernhart, R. Neuböck, and I. L. Hofacker, “The Vienna RNA Websuite,” *Nucleic Acids Res.*, vol. 36, no. Web Server issue, pp. W70–W74, July 2008, doi: 10.1093/nar/gkn188.

[33] A. T. Riley, J. M. Robson, and A. A. Green, “Generative and predictive neural networks for the design of functional RNA molecules,” July 14, 2023, *bioRxiv*. doi: 10.1101/2023.07.14.549043.

[34] I. Dotu, J. A. Garcia-Martin, B. L. Slinger, V. Mechery, M. M. Meyer, and P. Clote, “Complete RNA inverse folding: computational design of functional hammerhead ribozymes,” *Nucleic Acids Res.*, vol. 42, no. 18, pp. 11752–11762, Oct. 2014, doi: 10.1093/nar/gku740.

[35] J. A. Garcia-Martin and P. Clote, “RNA Thermodynamic Structural Entropy,” *PLoS ONE*, vol. 10, no. 11, p. e0137859, Nov. 2015, doi: 10.1371/journal.pone.0137859.

[36] A. Manzourolajdad and J. Arnold, “Secondary structural entropy in RNA switch (Riboswitch) identification,” *BMC Bioinformatics*, vol. 16, p. 133, Apr. 2015, doi: 10.1186/s12859-015-0523-2.

SUPPLEMENTARY INFORMATION A

NUCLEOTIDE SEQUENCES OF PLASMID CONSTRUCTS

Table A.1: Gene sequences and regulatory elements used in this study

Gene Name	**Sequence**
T7 promoter	TAATACGACTCACTATA
T7 terminator	TAGCATAACCCCTTGGGGCCT CTAAACGGGTCTTGAGGG GTTTTTTG
Chloramphenicol	ATGGAGAAAAAAATCACTGG ATATACCACCGTTGATATATC CCAATGGCATCGTAAAGAACA TTTTGAGGCATTTCAGTCAGTT GCTCAATGTACCTATAACCAG ACCGTTCAGCTGGATATTACG GCCTTTTTAAAGACCGTAAAG AAAAATAAGCACAAGTTTTAT CCGGCCTTTATTCACATTCTTG CCCGCCTGATGAATGCTCATC CGGAATTCCGTATGGCAATGA AAGACGGTGAGCTGGTGATAT GGGATAGTGTTCACCCTTGTT ACACCGTTTTCCATGAGCAAA CTGAAACGTTTTCATCGCTCTG GAGTGAATACCACGACGATTT CCGGCAGTTTCTACACATATA TTCGCAAGATGTGGCGTGTTA CGGTGAAAACCTGGCCTATTT CCCTAAAGGGTTTATTGAGAA TATGTTTTTCGTCTCAGCCAAT

	CCCTGGGTGAGTTTCACCAGT TTTGATTTAAACGTGGCCAAT ATGGACAACTTCTTCGCCCCC GTTTTCACCATGGGCAAATAT TATACGCAAGGCGACAAGGTG CTGATGCCGCTGGCGATTCAG GTTCATCATGCCGTCTGTGAT GGCTTCCATGTCGGCAGAATG CTTAATGAATTACAACAGTAC TGCGATGAGTGGCAGGGCGGG GCGTAA
Cat promoter	TGATCGGCACGTAAGAGGTTC CAACTTTCACCATAATGAAAT AAGATCACTACCGGGCGTATT TTTTGAGTTATCGAGATTTTCA GGAGCTAAGGAAGCTAAA
Superfolder GFP	ATGCGTAAAGGCGAAGAGCTG TTCACTGGTGTCGTCCCTATTC TGGTGGAACTGGATGGTGATG TCAACGGTCATAAGTTTTCCG TGCGTGGCGAGGGTGAAGGTG ACGCAACTAATGGTAAACTGA CGCTGAAGTTCATCTGTACTA CTGGTAAACTGCCGGTACCTT GGCCGACTCTGGTAACGACGC TGACTTATGGTGTTCAGTGCTT TGCTCGTTATCCGGACCATAT GAAGCAGCATGACTTCTTCAA GTCCGCCATGCCGGAAGGCTA TGTGCAGGAACGCACGATTTC CTTTAAGGATGACGGCACGTA CAAAACGCGTGCGGAAGTGA AATTTGAAGGCGATACCCTGG TAAACCGCATTGAGCTGAAAG GCATTGACTTTAAAGAAGACG GCAATATCCTGGGCCATAAGC TGGAATACAATTTTAACAGCC ACAATGTTTACATCACCGCCG ATAAACAAAAAAATGGCATTA AAGCGAATTTTAAAATTCGCC ACAACGTGGAGGATGGCAGC GTGCAGCTGGCTGATCACTAC CAGCAAAACACTCCAATCGGT GATGGTCCTGTTCTGCTGCCA GACAATCACTATCTGAGCACG CAAAGCGTTCTGTCTAAAGAT CCGAACGAGAAACGCGATCAT ATGGTTCTGCTGGAGTTCGTA ACCGCAGCGGGCATCACGCAT

	GGTATGGATGAACTGTACAAA TGA
rrnB T1 terminator	CAAATAAAACGAAAGGCTCA GTCGAAAGACTGGGCCTTTCG TTTTATCTGTTGTTTGTCGGTG AACGCTCTC
LacI promoter	GACACCATCGAATGGCGCAAA ACCTTTCGCGGTATGGCATGA TAGCGCCCGGAAGAGAGTCAA TTCAGGGTGGTGAAT
LacI	GTGAAACCAGTAACGTTATAC GATGTCGCAGAGTATGCCGGT GTCTCTTATCAGACCGTTTCCC GCGTGGTGAACCAGGCCAGCC ACGTTTCTGCGAAAACGCGGG AAAAAGTGGAAGCGGCGATG GCGGAGCTGAATTACATTCCC AACCGCGTGGCACAACAACTG GCGGGCAAACAGTCGTTGCTG ATTGGCGTTGCCACCTCCAGT CTGGCCCTGCACGCGCCGTCG CAAATTGTCGCGGCGATTAAA TCTCGCGCCGATCAACTGGGT GCCAGCGTGGTGGTGTCGATG GTAGAACGAAGCGGCGTCGA AGCCTGTAAAGCGGCGGTGCA CAATCTTCTCGCGCAACGCGT CAGTGGGCTGATCATTAACTA TCCGCTGGATGACCAGGATGC CATTGCTGTGGAAGCTGCCTG CACTAATGTTCCGGCGTTATTT CTTGATGTCTCTGACCAGACA CCCATCAACAGTATTATTTTCT CCCATGAAGACGGTACGCGAC TGGGCGTGGAGCATCTGGTCG CATTGGGTCACCAGCAAATCG CGCTGTTAGCGGGCCCATTAA GTTCTGTCTCGGCGCGTCTGC GTCTGGCTGGCTGGCATAAAT ATCTCACTCGCAATCAAATTC AGCCGATAGCGGAACGGGAA GGCGACTGGAGTGCCATGTCC GGTTTTCAACAAACCATGCAA ATGCTGAATGAGGGCATCGTT CCCACTGCGATGCTGGTTGCC AACGATCAGATGGCGCTGGGC GCAATGCGCGCCATTACCGAG TCCGGGCTGCGCGTTGGTGCG GATATCTCGGTAGTGGGATAC GACGATACCGAAGACAGCTCA

	TGTTATATCCCGCCGTTAACC ACCATCAAACAGGATTTTCGC CTGCTGGGGCAAACCAGCGTG GACCGCTTGCTGCAACTCTCT CAGGGCCAGGCGGTGAAGGG CAATCAGCTGTTGCCCGTCTC ACTGGTGAAAAGAAAAACCA CCCTGGCGCCCAATACGCAAA CCGCCTCTCCCCGCGCGTTGG CCGATTCATTAATGCAGCTGG CACGACAGGTTTCCCGACTGG AAAGCGGGCAGTGA
Ampicillin	ATGAGTATTCAACATTTCCGT GTCGCCCTTATTCCCTTTTTTG CGGCATTTTGCCTTCCTGTTTT TGCTCACCCAGAAACGCTGGT GAAAGTAAAAGATGCTGAAG ATCAGTTGGGTGCACGAGTGG GTTACATCGAACTGGATCTCA ACAGCGGTAAGATCCTTGAGA GTTTTCGCCCCGAAGAACGTT TTCCAATGATGAGCACTTTTA AAGTTCTGCTATGTGGCGCGG TATTATCCCGTATTGACGCCG GGCAAGAGCAACTCGGTCGCC GCATACACTATTCTCAGAATG ACTTGGTTGAGTACTCACCAG TCACAGAAAAGCATCTTACGG ATGGCATGACAGTAAGAGAAT TATGCAGTGCTGCCATAACCA TGAGTGATAACACTGCGGCCA ACTTACTTCTGACAACGATCG GAGGACCGAAGGAGCTAACC GCTTTTTTGCACAACATGGGG GATCATGTAACTCGCCTTGAT CGTTGGGAACCGGAGCTGAAT GAAGCCATACCAAACGACGA GCGTGACACCACGATGCCTGC AGCAATGGCAACAACGTTGCG CAAACTATTAACTGGCGAACT ACTTACTCTAGCTTCCCGGCA ACAATTAATAGACTGGATGGA GGCGGATAAAGTTGCAGGACC ACTTCTGCGCTCGGCCCTTCCG GCTGGCTGGTTTATTGCTGAT AAATCTGGAGCCGGTGAGCGT GGGTCTCGCGGTATCATTGCA GCACTGGGGCCAGATGGTAAG CCCTCCCGTATCGTAGTTATCT ACACGACGGGGAGTCAGGCA

	ACTATGGATGAACGAAATAGA CAGATCGCTGAGATAGGTGCC TCACTGATTAAGCATTGGTAA
f1 ori	ACGCGCCCTGTAGCGGCGCAT TAAGCGCGGCGGGTGTGGTGG TTACGCGCAGCGTGACCGCTA CACTTGCCAGCGCCCTAGCGC CCGCTCCTTTCGCTTTCTTCCC TTCCTTTCTCGCCACGTTCGCC GGCTTTCCCCGTCAAGCTCTA AATCGGGGGCTCCCTTTAGGG TTCCGATTTAGTGCTTTACGGC ACCTCGACCCCAAAAAACTTG ATTAGGGTGATGGTTCACGTA GTGGGCCATCGCCCTGATAGA CGGTTTTTCGCCCTTTGACGTT GGAGTCCACGTTCTTTAATAG TGGACTCTTGTTCCAAACTGG AACAACACTCAACCCTATCTC GGTCTATTCTTTTGATTTATAA GGGATTTTGCCGATTTCGGCC TATTGGTTAAAAAATGAGCTG ATTTAACAAAAATTTAACGCG AATTTTAACAAAATATTAACG TTTACAATTT

SUPPLEMENTARY INFORMATION B

LIST OF PRIMERS

Table B.1: Primer Sequences used for cloning of constructs

Primer Name	Sequence (5' -3')
AA-TN101	TAATACGACTCACTATAGGGG GGAT
AA-TN102	TCCTCTGTTCTAAAGTCCGTAC GTTCTTTCTATCATCCCCCCTA TAGTGAGTCGTATT
AA-TN103	ACGGACTTTAGAACAGAGGAG ATAAAGATGGTACGAAACCTG GCGGCAGCGCAA

AA-TN104	CCAGTGAACAGCTCTTCGCCTTTACGCATCTTTTGCGCTGCCGCCAGGTTT
AA-TN201	TATCGACGTCTAATACGACTCACTATAGGGAGCGTCTAC
AA-TN202	CCTCTGTTCTAAAGTCCGAGGACTGCAGCGTAGACGCTCCCTATAGTGAGTCGTATT
AA-TN203	AGTCCTCGGACTTTAGAACAGAGGAGATAAAGATGGAGGATAACCTGGCGGCAGCGCAA
AA-TN204	ACCAGTGAACAGCTCTTCGCCTTTACGCATCTTTTGCGCTGCCGCCAGGTTA
AA-TN301	TATCGACGTCTAATACGACTCACTATAGGGAGTCAGAGGTGACAAGATTGGGGACTT
AA-TN302	CCAGGTTGATTGGCATCTTTATCTCCTCTGTTCTAAAGTCCCCAATCTTGTCACCTCTGA
AA-TN303	GGAGATAAAGATGCCAATCAACCTGGCGGCAGCGCAAAAGATGCGTAA
AA-TN304	ACCAGTGAACAGCTCTTCGCCTTTACGCATCTTTTGCGCTGCCG
AA-TN401	TATCGACGTCTAATACGACTCACTATAGGGGGCCTGACGGGAT
AA-TN402	ACATCTTTATCTCCTCTGTTCTAAAGTCCTTTCTATCATCCCGTCAGGCCCCCTA
AA-TN403	AAAGGACTTTAGAACAGAGGAGATAAAGATGTTTCTCAACCTGGCGGCAGCGCAAA
AA-TN404	ACCAGTGAACAGCTCTTCGCCTTTACGCATCTTTTGCGCTGCCGCCAGGTT
AA-TN501	TATCGACGTCTAATACGACTCACTATAGGGCCATGAGAGCCTCAA
AA-TN502	TCTCCTCTGTTCTAAAGTCCCAGATCTTGAGGCTCTCATGGCCCTA
AA-TN503	GATCTGGGACTTTAGAACAGAGGAGATAAAGATGCAGATTAACCTGGCGGCAGCGCAAA

AA-TN504	ACCAGTGAACAGCTCTTCGCC TTTACGCATCTTTTGCGCTGCC GCCAGGTTA
AA-TN601	TATCGACGTCTAATACGACTC ACTATAGGGGAGCGTGAACAC AAATC
AA-TN602	CCTAACATCTTTATCTCCTCTG TTCTAAAGTCCTTAGGATTTGT GTTCACGCTCCCCT
AA-TN603	GGACTTTAGAACAGAGGAGAT AAAGATGTTAGGAAACCTGGC GGCAGCGCAAAAGATGC
AA-TN604	ACCAGTGAACAGCTCTTCGCC TTTACGCATCTTTTGCGCTGCC G
AA_1-1	GGGGCAAAGACACTTTCCAGT CTCTGCGGACTTTAGAACAGA GGAGATA
AA_1-2	CTTTTGCGCTGCCGCCAGGTTC GTCTCTGCCATCTTTATCTCCT CTGTTCTAAAGTCCG
AA_2-1	GGGCTGCAAAGACACTTTCCA GTCTCTGGACTTTAGAACAGA GGAGATAAAGATG
AA_2-2	CTTTTGCGCTGCCGCCAGGTTC CAGTCTCTCATCTTTATCTCCT CTGTTCTAAAGTCC
AA_3-1	GGGCTGTTCCATAGCCTTTGC CGTAGTGGACTTTAGAACAGA GGAGATAAAGATGA
AA_3-2	CTTTTGCGCTGCCGCCAGGTTT GCCGTAGTCATCTTTATCTCCT CTGTTCTAAAGTCCAC
AA_SW-BB	CGGTAGTGATCTTATTTCATTA TGG
pAA_New_01	TATCGACGTCTAATACGACTC ACTATAGGGTACGTTTCGACC TCGGT
pAA_New_02	AGAAGACATGTTGTTTATTTTC TCCTCTTTAAATCTTCTAACCG AGGTCGAAACGTACCC
pAA_New_03	GAAGATTTAAAGAGGAGAAA ATAAACAACATGTCTTCTAAC AACCTGGCGGCAGCGCAAA
pAA_New_04	ACCAGTGAACAGCTCTTCGCC TTTACGCATCTTTTGCGCTGCC GCCA

pAA_New15_01	TATCGACGTCTAATACGACTC ACTATAGGGACGTTTCGACCT CGGTTA
pAA_New15_02	GAAGACCCATGTTGTTTATTTT CTCCTCTTTATAGTCTTCTAAC CGAGGTCGAAACGTCC
pAA_New15_03	AAGAGGAGAAAATAAACAAC ATGGGTCTTCTAAAACCTGGC GGCAGCGCAAA
pAA_New15_04	ACCAGTGAACAGCTCTTCGCC TTTACGCATCTTTTGCGCTGCC GCCA
PrimerAA_10	CCCTATAGTGAGTCGTATTAG ACGTC
PrimerAA_11	ATGCGTAAAGGCGAAGAGCTG
PrimerAA_12	CCCTATAGTGAGTCGTATTAA TTTCGCGG
PrimerAA_13	TAGCATAACCCCTTGGGGCCT CTAAAC
AA_forTruncated	TGCCGGCCACGATGCGTCCGG CGTA
AA_TrunLac_01	CCCGTTTAGAGGCCCCAAGGG GTTATGCTATAGCCATTCCAT GAGAGCCTCAAGATCTGT
AA_TrunLac_02	GACTGGAAAGTGTCTTTGCAG GAAAGAACACAGATCTTGAGG CTCTCATGGAATG
AA_TrunLac_03	TCCTGCAAAGACACTTTCCAG TCTCTGCGCGATCTCGGCTTTG AGGGGGCCTGA
AA_TrunLac_04	TCTTCTAACCGAGGTCGAAAC GTACGTTCTTTCTATCATCCCG TCAGGCCCCCTCAAAGC
AA_TrunLac_05	CGTTTCGACCTCGGTTAGAAG ACTCATGGAATTGTTATCCGC TCACAATTCCCCTATAGT
AA_TrunLac_06	TCCCGCGAAATTAATACGACT CACTATAGGGGAATTGTGAGC GGA
pAA_Trial1_01	TATCGACGTCTAATACGACTC ACTATAGGGAAGAACGTACGT TTCGACCTCGGTTA
pAA_Trial1_02	TCTCCTCTGTTCTAAAGTCCAT GAGTCTTCTAACCGAGGTCGA AACGTACGTTCTTCC
pAA_Trial1_03	GACTCATGGACTTTAGAACAG AGGAGATAAAGATGATGAGTC TTCTAAACCTGGCGGCAGCGC AA

pAA_Trial1_04	GAATAGGGACGACACCAGTG AACAGCTCTTCGCCTTTACGC ATCTTTTGCGCTGCCGCCA
PAA_New17_01	TATCGACGTCTAATACGACTC ACTATAGGGCAAAGCGTCTAC GCTGCAGT
PAA_New17_02	GTCCTCCATGTTGTTTATTTTC TCCTCTTTATAGAGGACTGCA GCGTAGACGCTTTGCCC
PAA_New17_03	AAAGAGGAGAAAATAAACAA CATGGAGGACTGTAACCTGGC GGCAGCGCAAAAGATGC
PAA_New17_04	ACCAGTGAACAGCTCTTCGCC TTTACGCATCTTTTGCGCTGCC G
PAA_New28_01	TATCGACGTCTAATACGACTC ACTATAGGGGCCATTCCATGA GAGCCTCAAGATT
PAA_New28_02	CCTCAAGATCATGTTGTTTATT TTCTCCTCTTTAAAATCTTGAG GCTCTCATGGAATGGC
PAA_New28_03	AAAGAGGAGAAAATAAACAA CATGATCTTGAGGAACCTGGC GGCAGCGCAAAAGATGC
PAA_New28_04	ACCAGTGAACAGCTCTTCGCC TTTACGCATCTTTTGCGCTGCC G
PAA_New40_01	TATCGACGTCTAATACGACTC ACTATAGGGTCTACGCTGCAG TCCTCGCTCACTT
PAA_New40_02	CGCTCACTCATGTTGTTTATTT TCTCCTCTTTAAAAGTGAGCG AGGACTGCAGCGTAG
PAA_New40_03	AGGAGAAAATAAACAACATG AGTGAGCGAAACCTGGCGGCA GCGCAAAAGATGCGTAA
PAA_New41_01	TATCGACGTCTAATACGACTC ACTATAGGGGCCTGACGGGAT
PAA_New41_02	GAACCATGTTGTTTATTTTCTC CTCTTTAAAGTTCTTTCTATCA TCCCGTCAGGCCCCTA
PAA_New41_03	AGAACTTTAAAGAGGAGAAA ATAAACAACATGGTTCTTTCC AACCTGGCGGCAGCGCAAA
PAA_New41_04	ACCAGTGAACAGCTCTTCGCC TTTACGCATCTTTTGCGCTGCC GCCA

SUPPLEMENTARY INFORMATION C

CONSTRUCT PLASMID MAPS

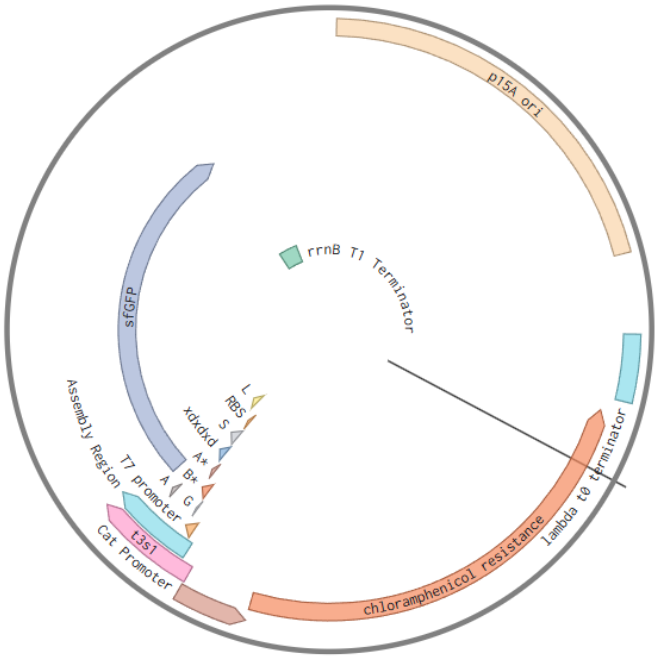

Figure C.1: The schematic illustration of pZa sfGFP M-influenza_switch7

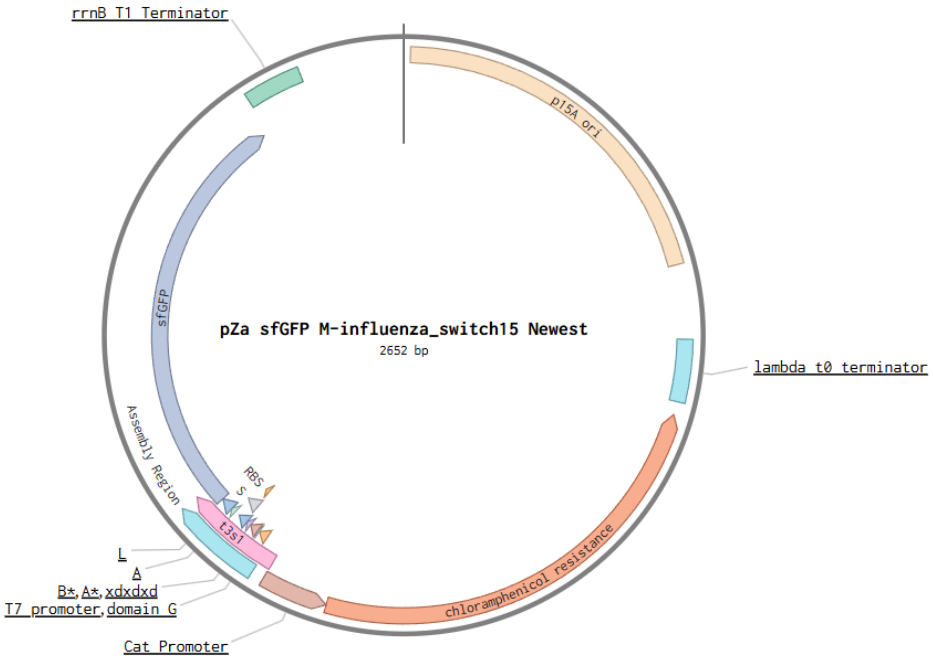

Figure C.2: The schematic illustration of pZa sfGFP M-influenza_switch8

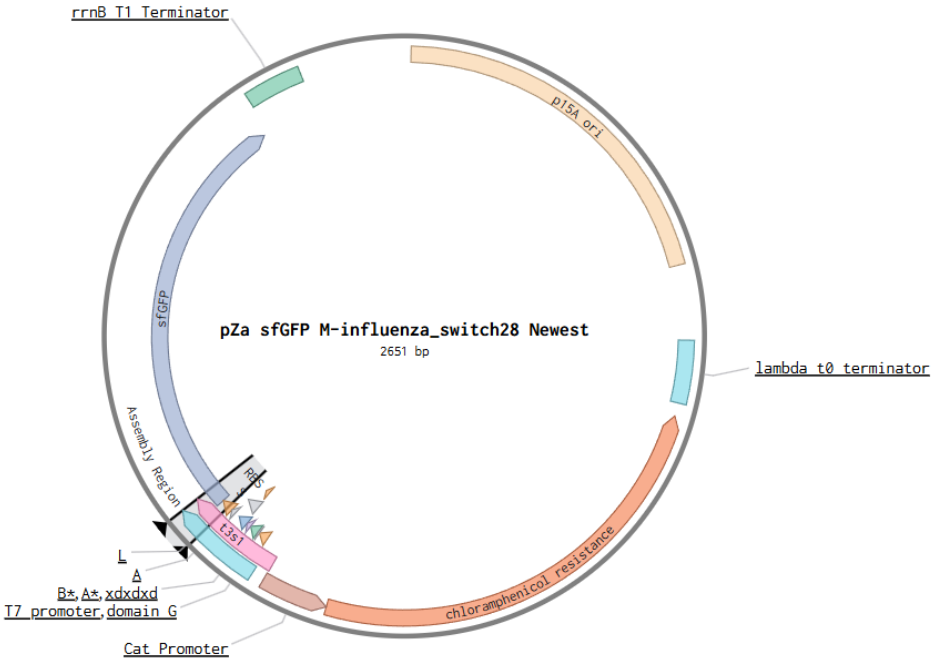

Figure C.3: The schematic illustration of pZa sfGFP M-influenza_switch9

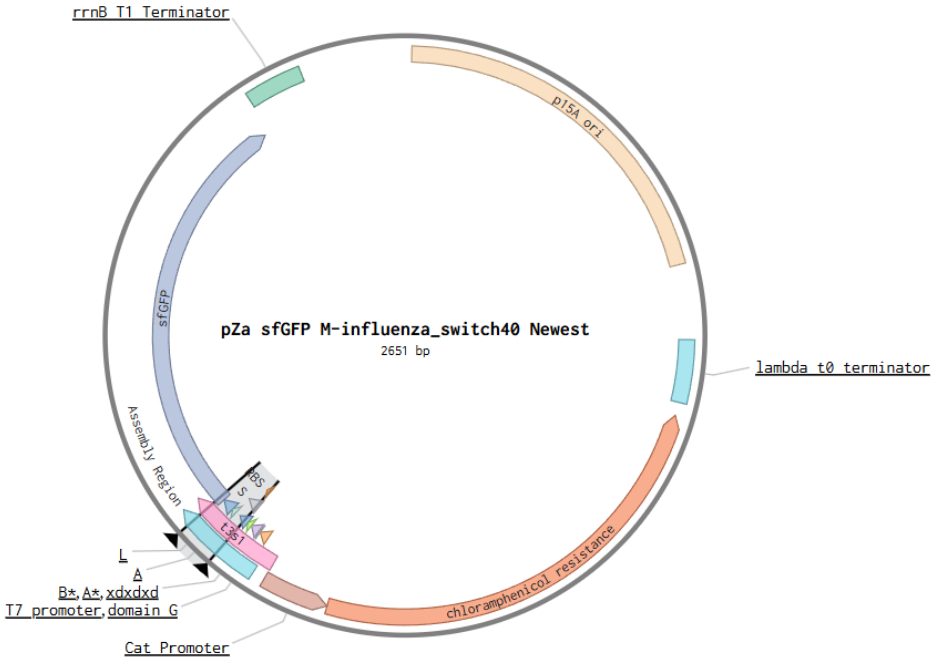

Figure C.4: The schematic illustration of pZa sfGFP M-influenza_switch10

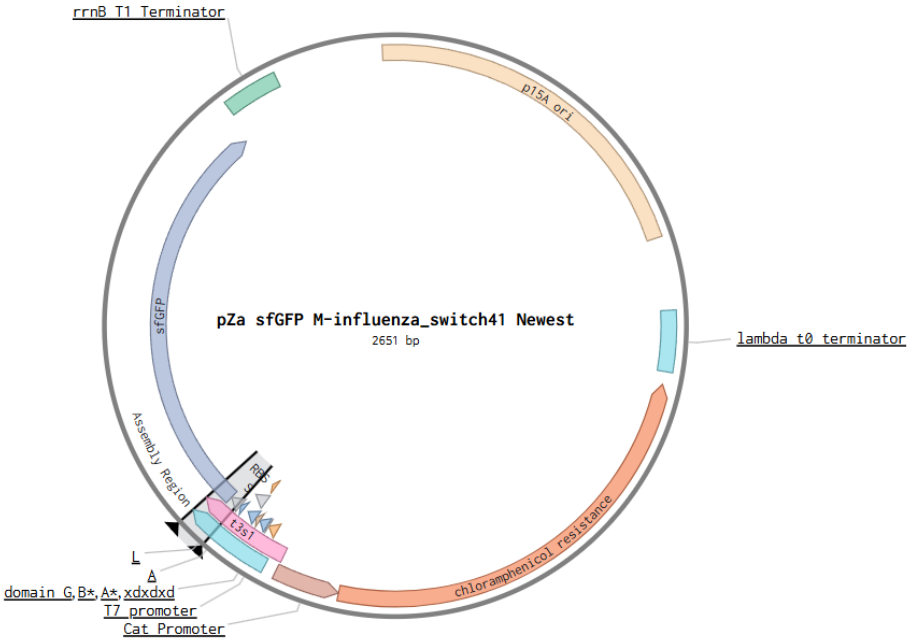

Figure C.5: The schematic illustration of pZa sfGFP M-influenza_switch11

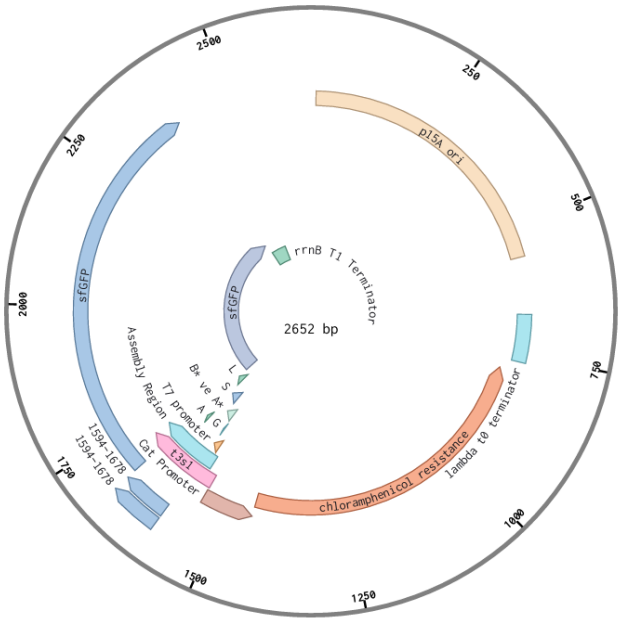

Figure C.6: The schematic illustration of pZa sfGFP M-influenza_switch12

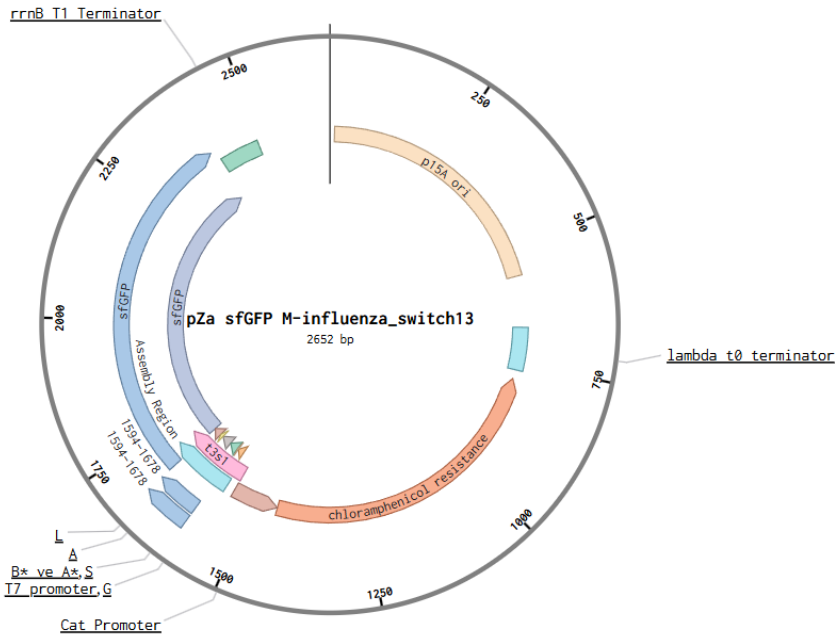

Figure C.7: The schematic illustration of pZa sfGFP M-influenza_switch13

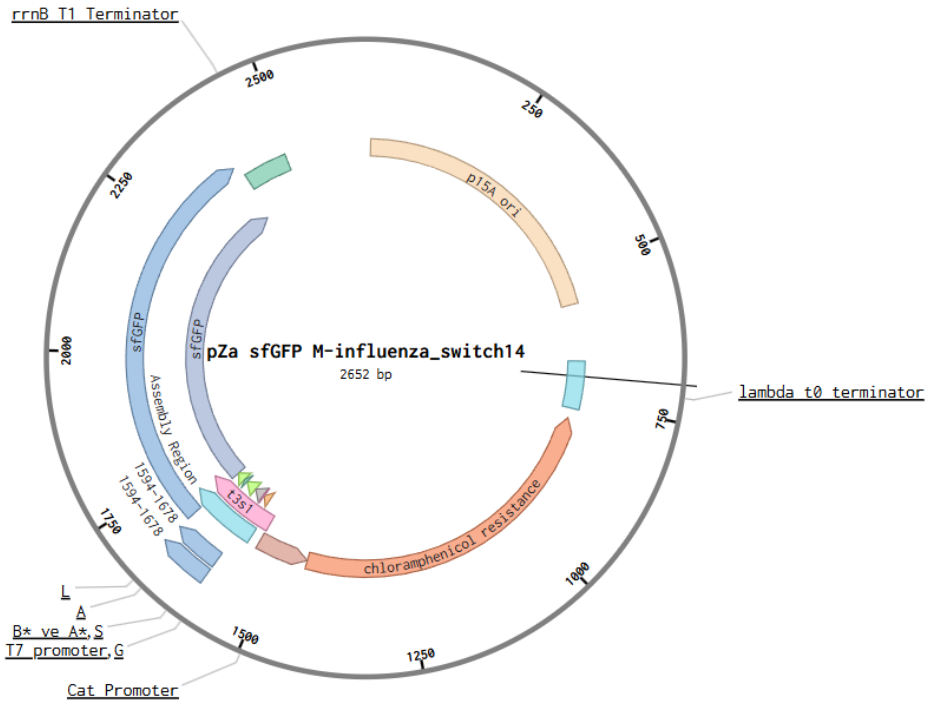

Figure C.8: The schematic illustration of pZa sfGFP M-influenza_switch14

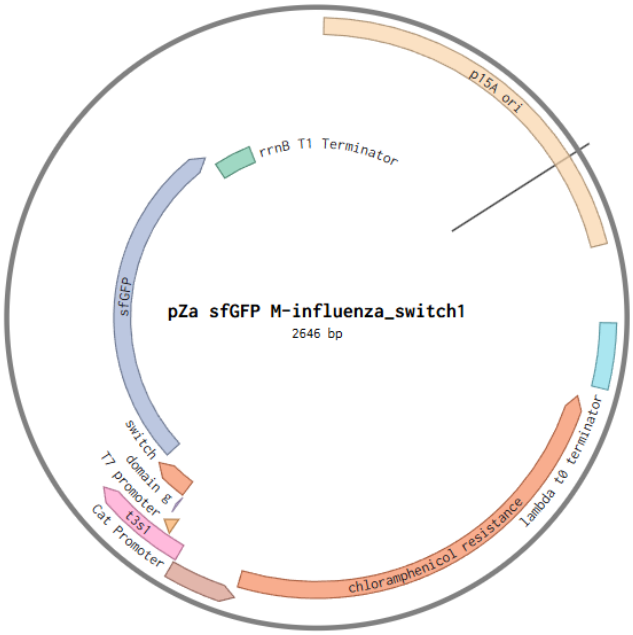

Figure C.9: The schematic illustration of pZa sfGFP M-influenza_switch1

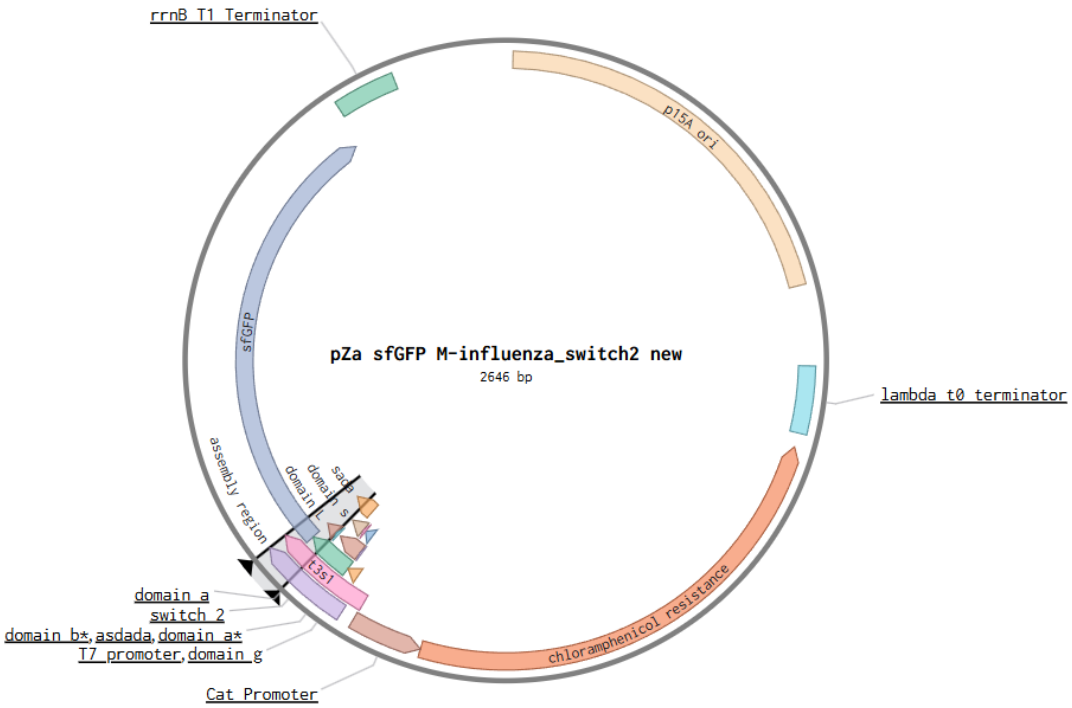

Figure C.10: The schematic illustration of pZa sfGFP M-influenza_switch2

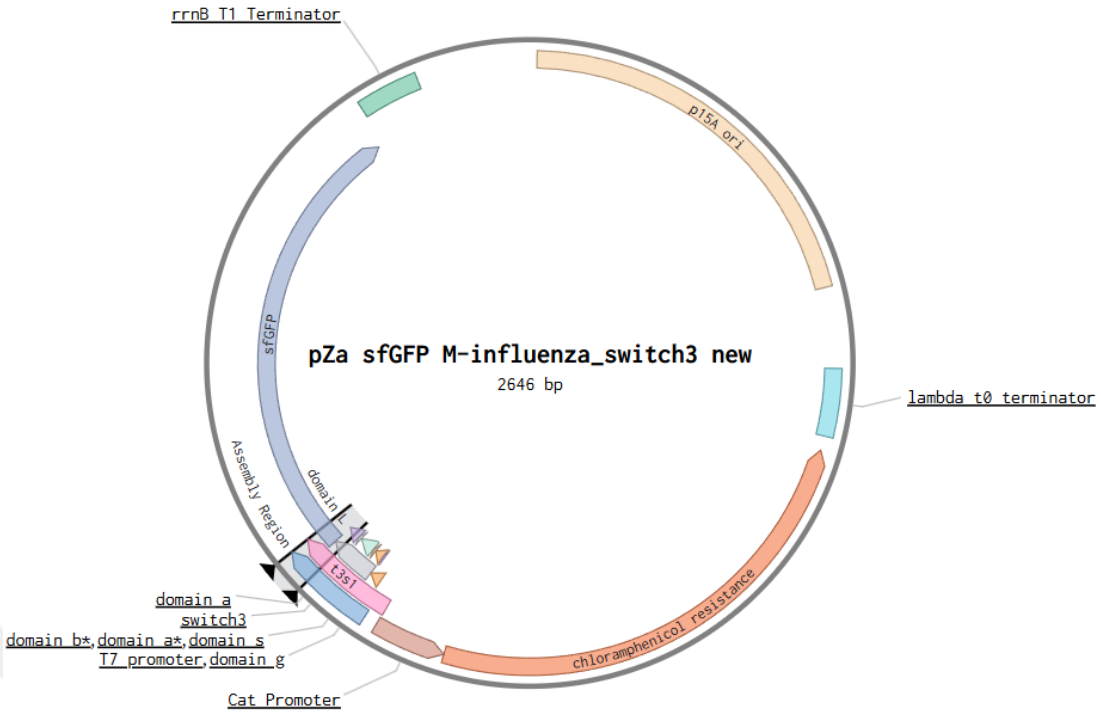

Figure C.11: The schematic illustration of pZa sfGFP M-influenza_switch3

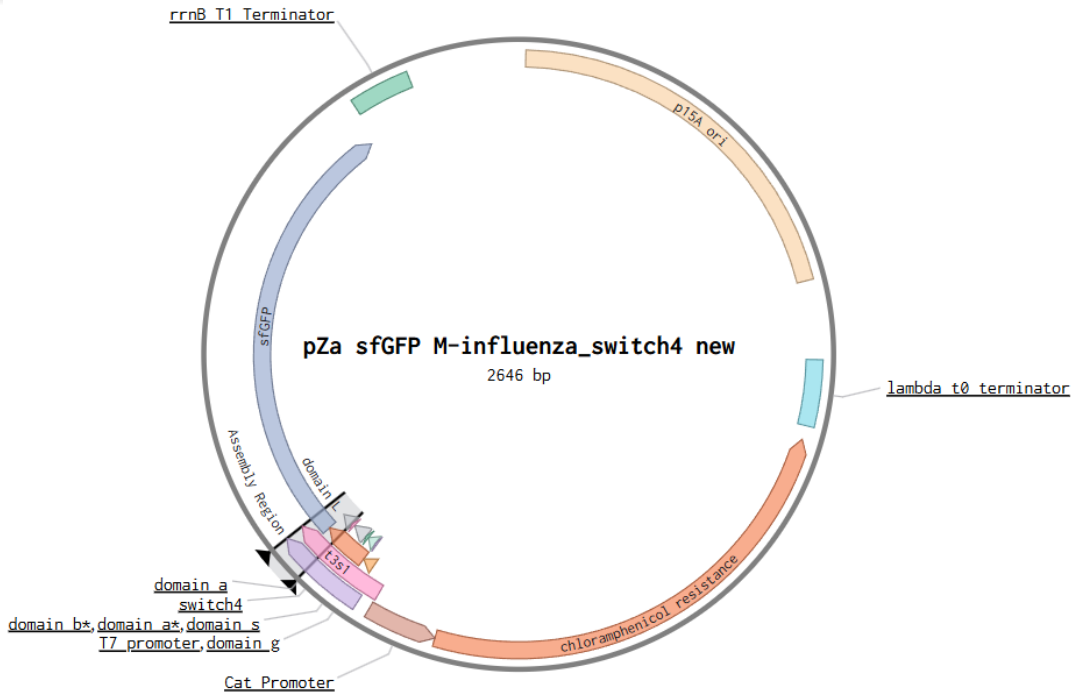

Figure C.12: The schematic illustration of pZa sfGFP M-influenza_switch4

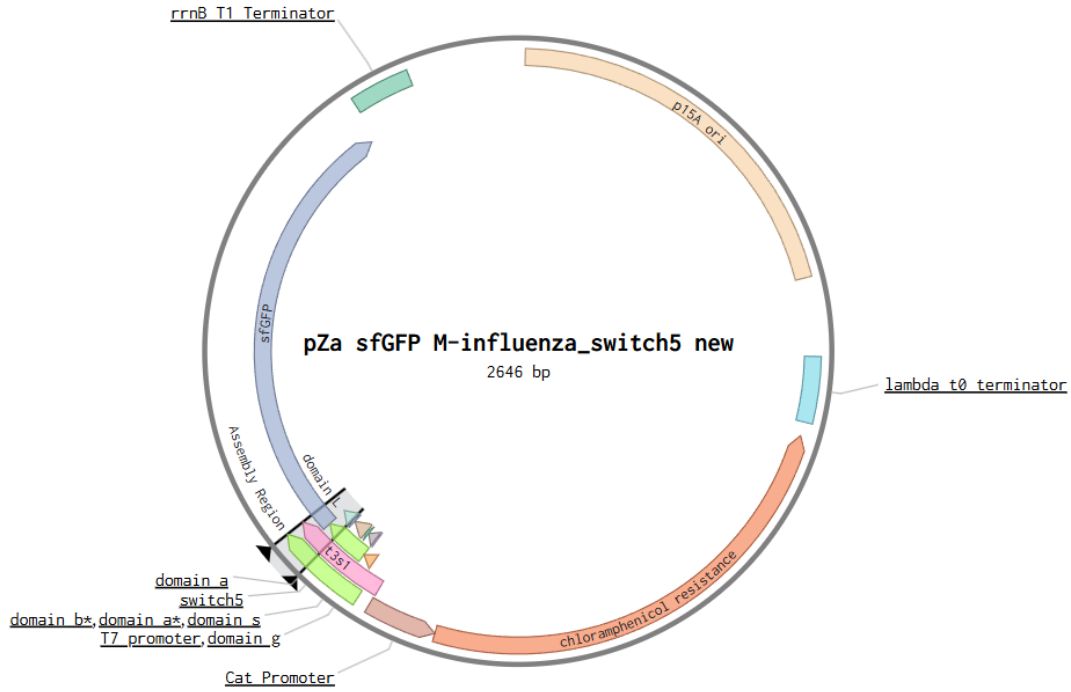

Figure C.13: The schematic illustration of pZa sfGFP M-influenza_switch5

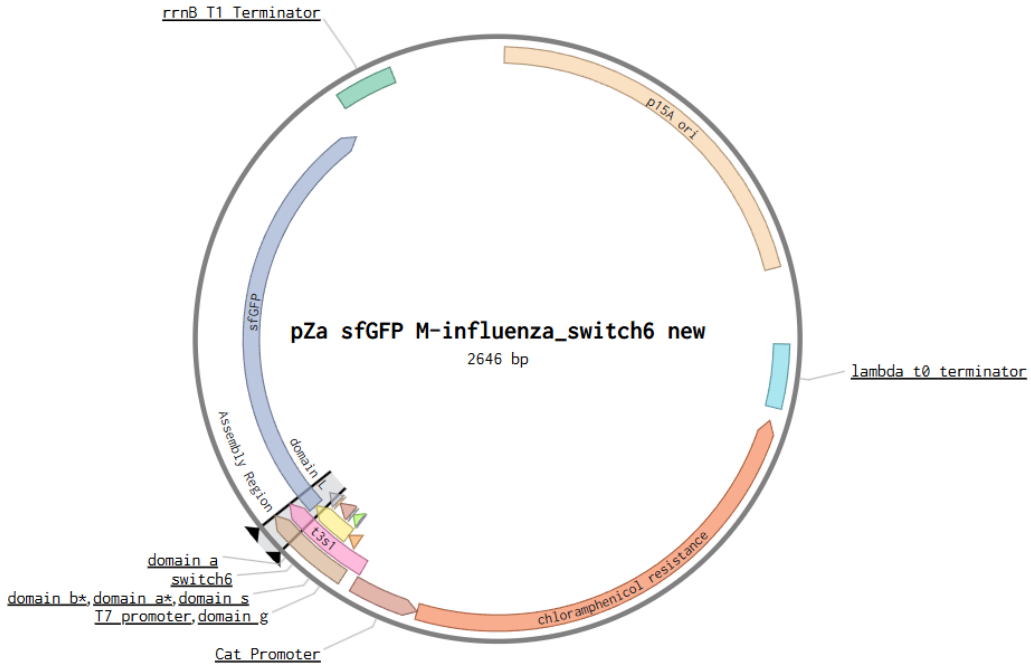

Figure C.14: The schematic illustration of pZa sfGFP M-influenza_switch6

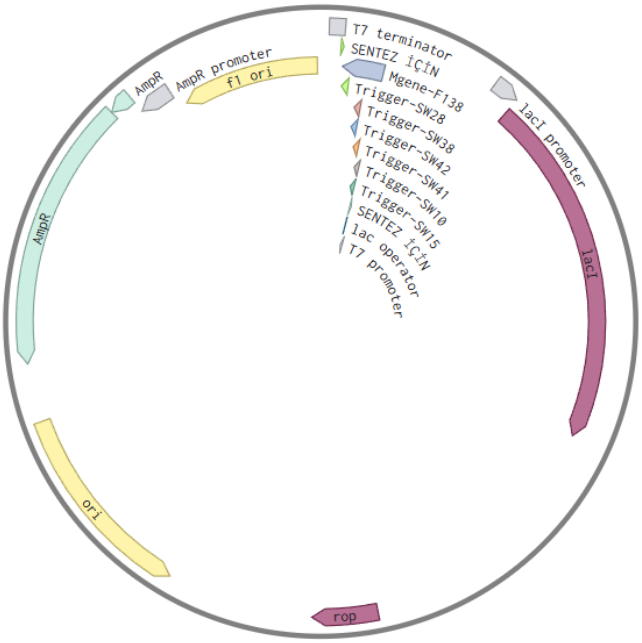

Figure C.15: The schematic illustration of pET-22b(+)- M gene_Influenza_trigger_truncated

SUPPLEMENTARY INFORMATION D

VERIFICATION OF CONSTRUCTS VIA SEQUENCING

Sanger sequencing was conducted for sequence analysis. To facilitate the identification of mismatched bases, the resulting sequence was analyzed and aligned using Benchling to compare the matching status of the plasmid sequence.

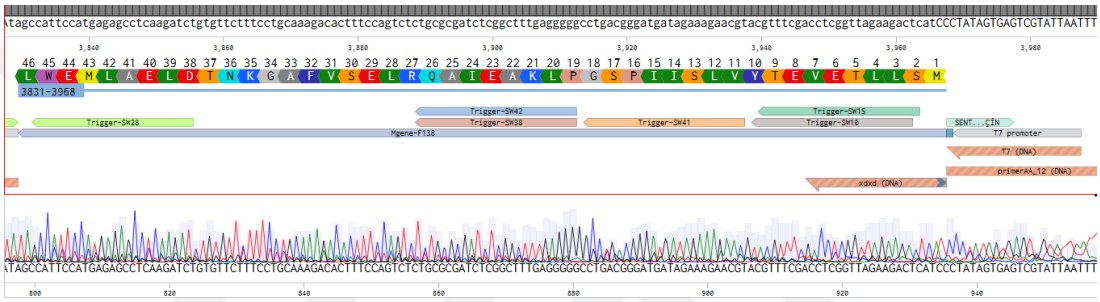

Figure D.1: Sequencing results of pET-22b(+) -M gene_Influenza_trigger newly (truncated)

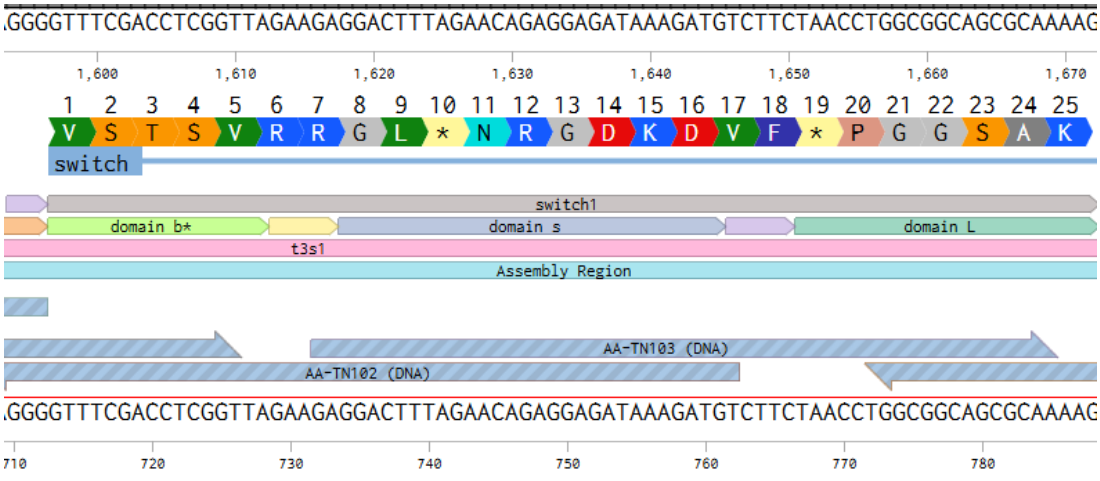

Figure D.2: Sequencing results of pZa sfGFP M-Influenza_switch10 Newest

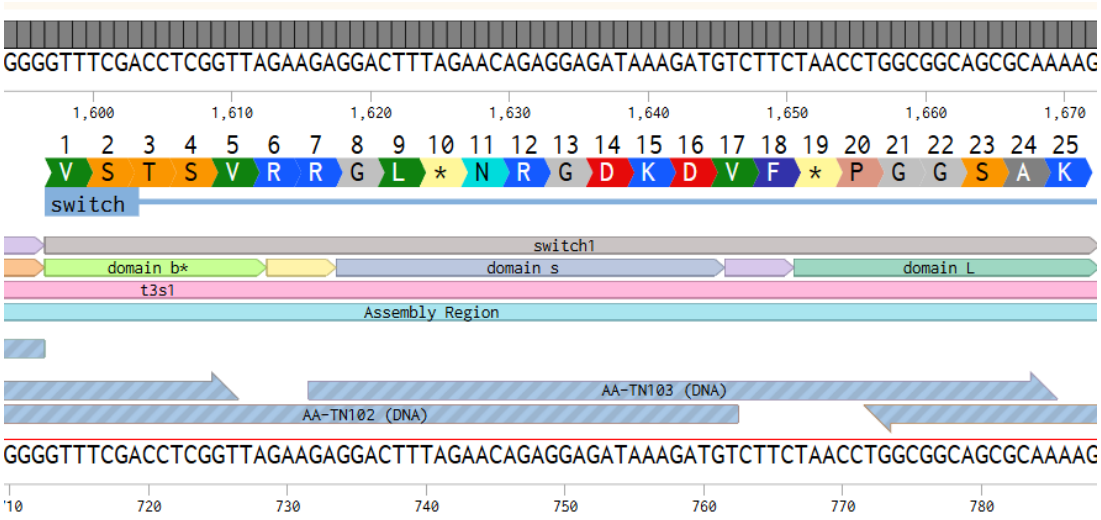

Figure D.3: Sequencing results of pZa sfGFP M_Influenza_swith15 Newest

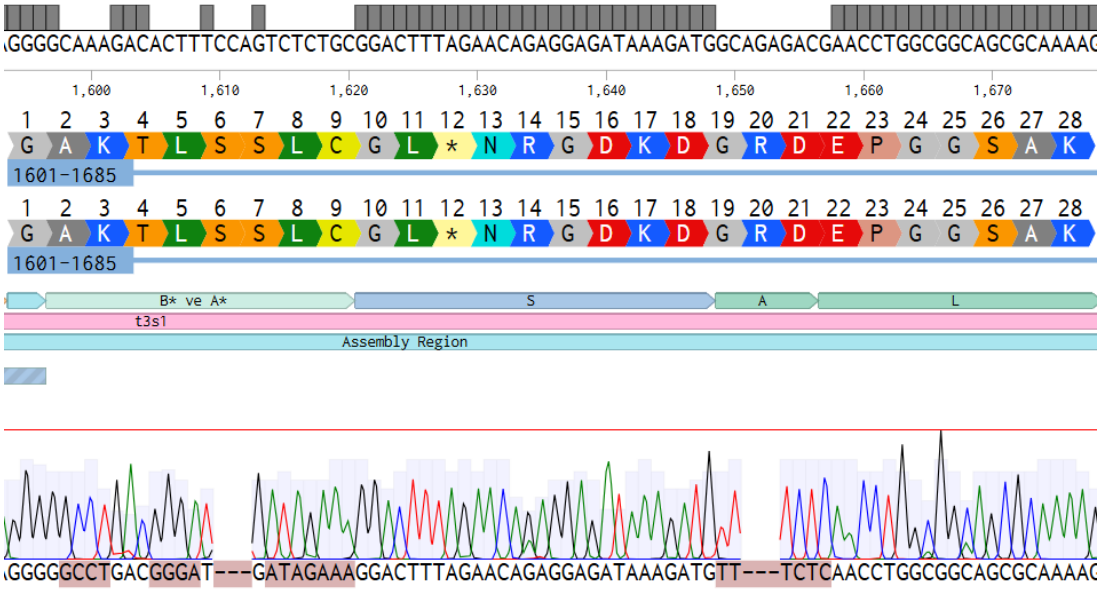

Figure D.4: Sequencing results of SW-1. Due to the folding of the toehold domain, the region where it is located may remain in a closed conformation, which could hinder efficient translation

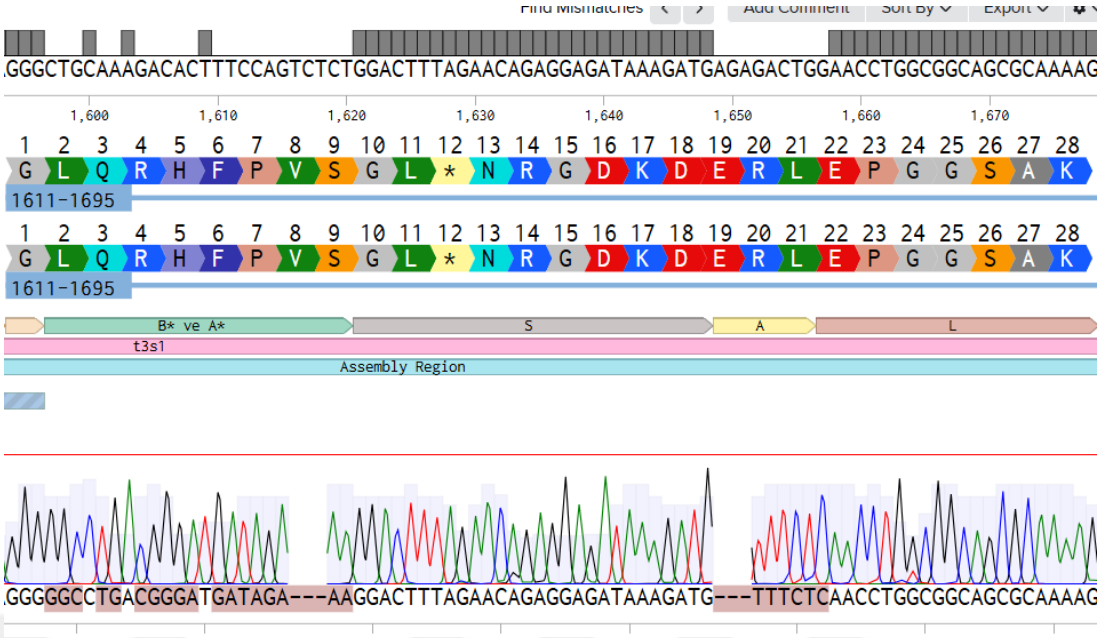

Figure D.5: Sequencing results of SW-2. Due to the folding of the toehold domain, the region where it is located may remain in a closed conformation, which could hinder efficient translation

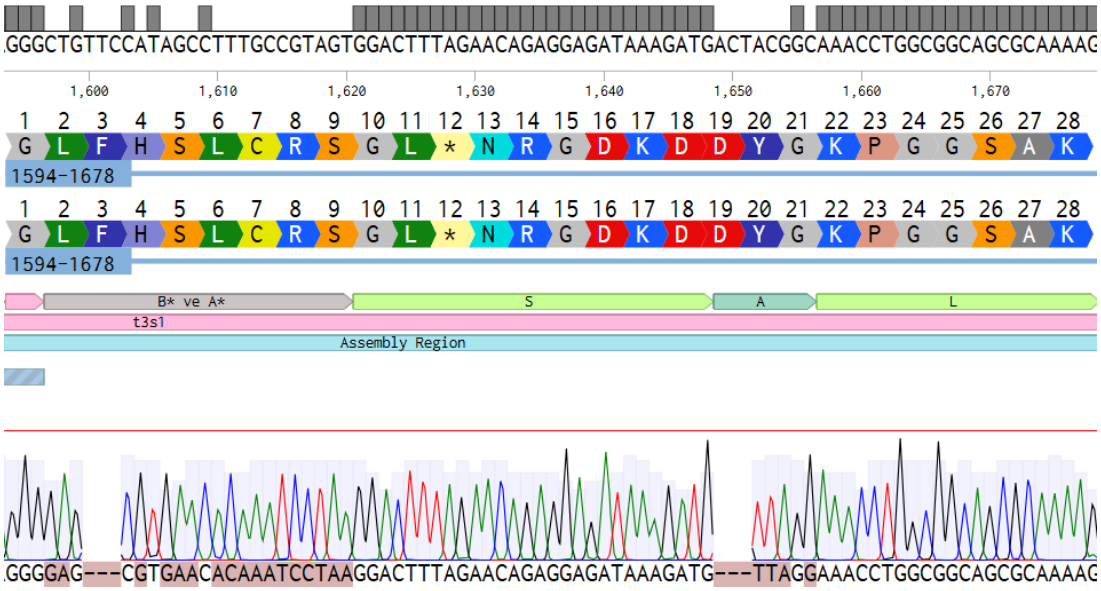

Figure D.6: Sequencing results of SW-3. Due to the folding of the toehold domain, the region where it is located may remain in a closed conformation, which could hinder efficient translation

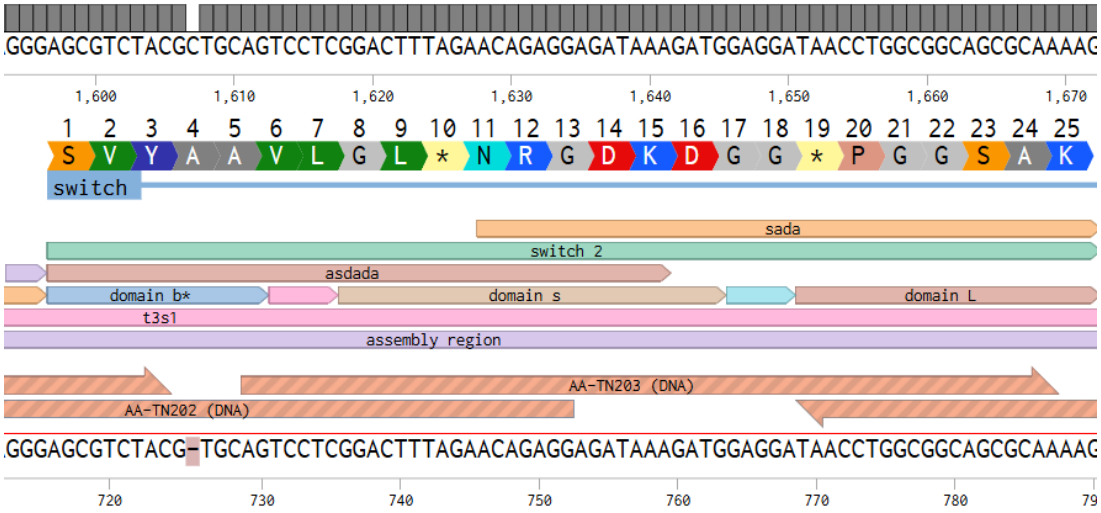

Figure D.7: Sequencing results of pZa sfGFP M-influenza_switch2 new

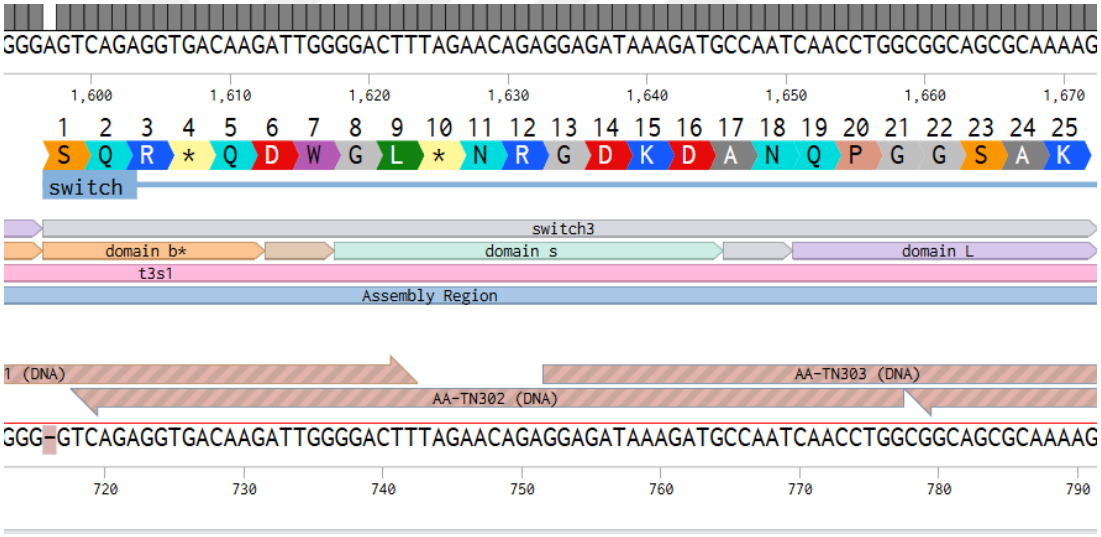

Figure D.8: Sequencing results of pZa sfGFP M-influenza_switch3 new

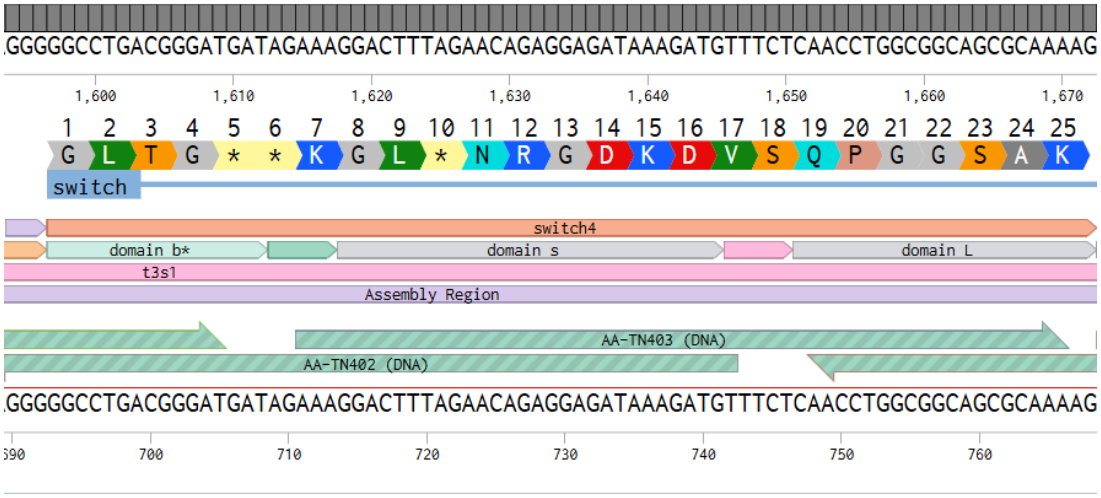

Figure D.9: Sequencing results of pZa sfGFP M-influenza_switch4 new

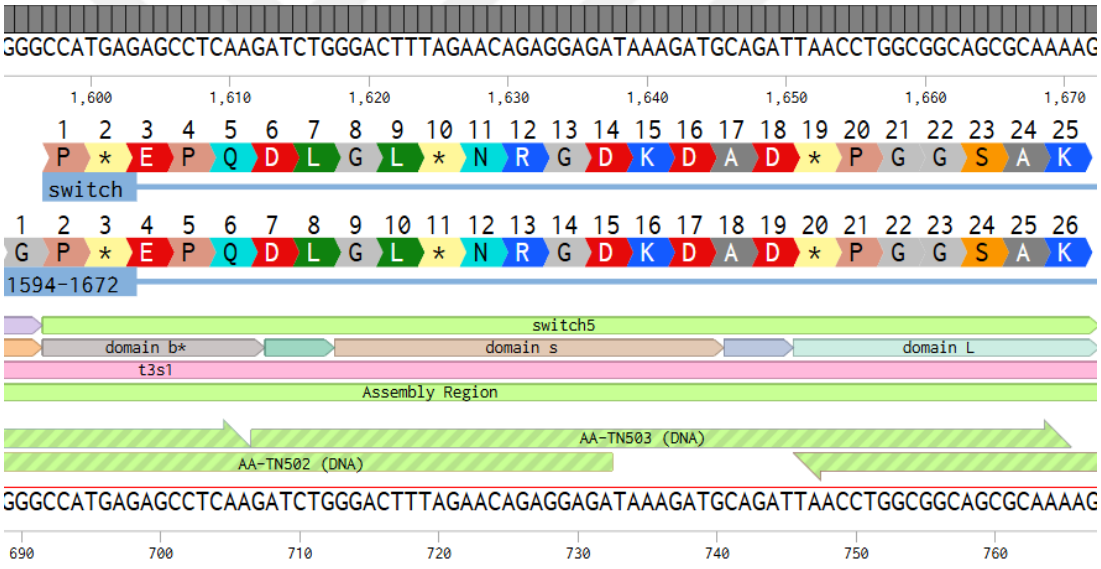

Figure D.10: Sequencing results of pZa sfGFP M-influenza_switch5 new

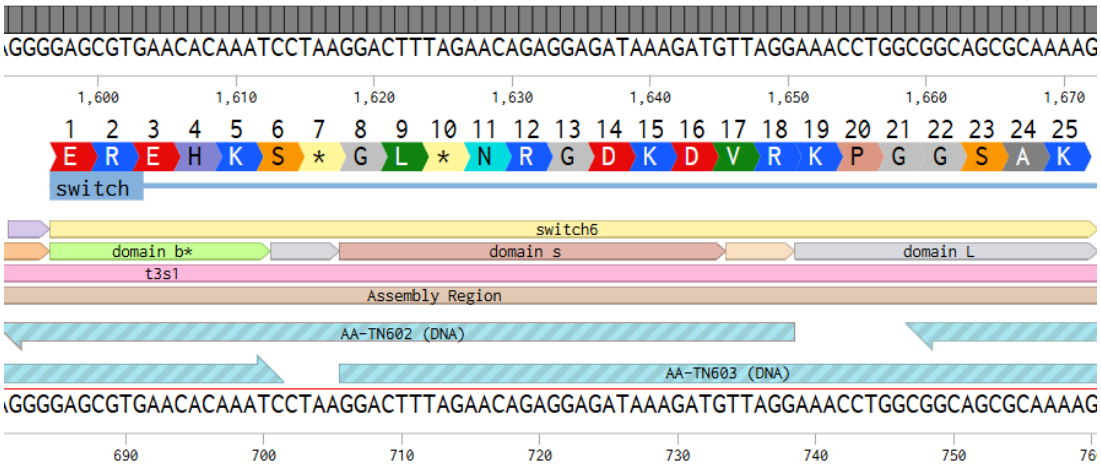

Figure D.11: Sequencing results of pZa sfGFP M-influenza_switch6 new

SUPPLEMENTARY INFORMATION E

ADDITIONAL REACTION RECIPES

Table E.1: Lysogeny Broth (LB) Growth Medium

Component	**Amount**
Yeast Extract	5 g
Tryptone	10 g
Sodium Chloride (NaCl)	10 g
Water	1000 mL

Table E. 1: Lysogeny Broth (LB) Growth Medium

Table E.2: TSS Buffer Recipe

Component	**Amount**
PEG 8000	5 g
2.5 mL DMSO	2.5 mL
1M $MgCl_2$	1.5 mL
LB Medium	Up to 50 mL

Table E. 2: TSS Buffer Recipe

Table E.3: Lysogeny Broth (LB) Agar Recipe

Component	**Amount**
Yeast Extract	5 g
Tryptone	10 g
Sodium Chloride (NaCl)	10 g
Agar	15 g
Water	1000 mL

Table E. 3: Lysogeny Broth (LB) Agar

Table E.4: PCR reaction mix recipe with Q5

Component	**Amount**
5X Q5 Reaction Buffer	5 µl
10 mM dNTP	0.5 µl
10 µM Forward Primer	1.25 µl
10 µM Reverse Primer	1.25 µl
Template DNA	0.5 ng – 0.5 µg
Q5 DNA Polymerase	0.5 µl
Nuclease Free Water	Up to 25 µl

Table E. 4: PCR reaction mix recipe with Q5

Table E.5: Gibson Assembly Mixture (1.33x)

Component	**Amount**
Taq Ligase (40 U/µl)	50 µl
5X Isothermal Buffer	100 µl
T5 Exonuclease (1 U/µl)	2 µl
Phusion Polymerase	6.25 µl
Nuclease Free Water	216.75 µl

Table E.5: Gibson Assembly Mixture

Table E.6: 10x PBS (pH 7.4)

Component	**Amount**
Na_2HPO_4	14.4 g
KH_2PO_4	2.4 g

NaCl	80 g
KCl	2 g
Nuclease Free Water	To 1000 mL

Table E. 6: 10x PBS (pH 7.4)